nature immunology

Article

https://doi.org/10.1038/s41590-024-02062-x

Differential roles of human CD4$^+$ and CD8$^+$ regulatory T cells in controlling self-reactive immune responses

Received: 26 April 2024

Accepted: 10 December 2024

Published online: 13 January 2025

Check for updates

Xin Chen[1,6], Mustafa Ghanizada[1,2,6], Vamsee Mallajosyula[1], Elsa Sola[1], Robson Capasso[3], Karan Raj Kathuria[1] & Mark M. Davis[1,4,5]

Here we analyzed the relative contributions of CD4$^+$ regulatory T cells expressing Forkhead box protein P3 (FOXP3) and CD8$^+$ regulatory T cells expressing killer cell immunoglobulin-like receptors to the control of autoreactive T and B lymphocytes in human tonsil-derived immune organoids. *FOXP3* and *GZMB* respectively encode proteins FOXP3 and granzyme B, which are critical to the suppressive functions of CD4$^+$ and CD8$^+$ regulatory T cells. Using CRISPR–Cas9 gene editing, we were able to achieve a reduction of ~90–95% in the expression of these genes. *FOXP3* knockout in tonsil T cells led to production of antibodies against a variety of autoantigens and increased the affinity of influenza-specific antibodies. By contrast, *GZMB* knockout resulted in an increase in follicular helper T cells, consistent with the ablation of CD8$^+$ regulatory T cells observed in mouse models, and a marked expansion of autoreactive CD8$^+$ and CD4$^+$ T cells. These findings highlight the distinct yet complementary roles of CD8$^+$ and CD4$^+$ regulatory T cells in regulating cellular and humoral responses to prevent autoimmunity.

How the immune system maintains tolerance to self-antigens while having the ability to launch vigorous responses to foreign antigens has been a central question in immunology since Paul Ehrlich first raised it in 1901 (ref. 1). After some false starts, the modern era of investigations into this question emerged with analyses of B cell tolerance by Goodnow[2] and the discovery, by Sakaguchi and colleagues, of a CD4$^+$ T cell subset expressing the transcription factor FOXP3 that has been shown to have a major role in preventing autoimmunity[3,4]. More recently, a small subset of CD8$^+$ T cells in mice was found by Cantor and colleagues to be another T cell subset involved in controlling autoreactivity[5–7]. Work by our group[8,9] has shown that these T cells have a critical role in preventing autoimmunity following infection and have elevated levels in human autoimmune diseases. These CD8$^+$ T cells express genes encoding members of the Ly49 family in mice and killer cell immunoglobulin-like receptors (KIRs) in humans and are notably active during infectious diseases; evidence suggests that they are specifically tasked with controlling self-reactive T cells that have been activated by infection[8]. Thus, at least two major types of regulatory T (T_{reg}) cell maintain tolerance, but their specific roles have not been explored extensively.

To address this question, we used our recently established human tonsil organoid system[10]. In response to stimulation with influenza and other vaccines, this system recapitulates the processes of somatic hypermutation, affinity maturation and B cell maturation and produces antigen-specific antibodies[10,11]. Here, we disabled each of the tonsillar CD4$^+$ and CD8$^+$ T_{reg} cells by knockout (KO) of key genes related to

[1]Institute for Immunity, Transplantation, and Infection, Stanford University, Stanford, CA, USA. [2]Department of Immunology and Microbiology, University of Copenhagen, Copenhagen, Denmark. [3]Division of Sleep Surgery, Department of Otolaryngology-Head and Neck Surgery, Stanford University School of Medicine, Stanford, CA, USA. [4]Department of Microbiology and Immunology, Stanford University School of Medicine, Stanford, CA, USA. [5]The Howard Hughes Medical Institute, Stanford University School of Medicine, Stanford, CA, USA. [6]These authors contributed equally: Xin Chen, Mustafa Ghanizada. e-mail: mmdavis@stanford.edu

https://doi.org/10.1038/s41590-024-02062-x

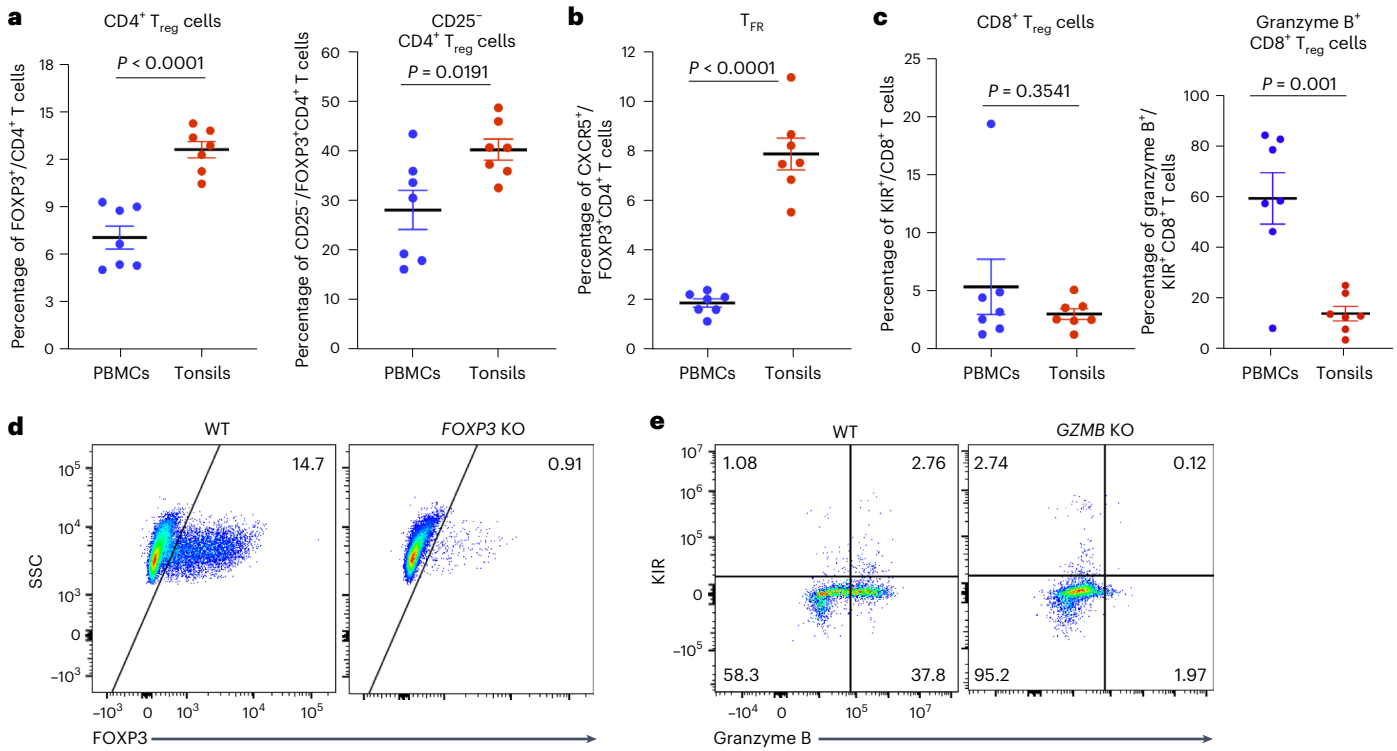

Fig. 1 | CD4$^+$ and CD8$^+$ T$_{reg}$ cell subsets in human tonsils showed percentage and phenotypic differences compared with peripheral blood. a–**c**, Percentages of CD4$^+$ T$_{reg}$ cells (CD4$^+$FOXP3$^+$) and CD25$^-$CD4$^+$ T$_{reg}$ cells (**a**), follicular T$_{reg}$ cells (T$_{FR}$; CXCR5$^+$FOXP3$^+$) (**b**), and CD8$^+$ T$_{reg}$ cells (KIR$^+$CD8$^+$) and granzyme$^+$CD8$^+$ T$_{reg}$ cells (**c**) from blood and tonsil samples from age- and gender-matched donors ($n = 7$). **d**,**e**, Representative FACS plots of FOXP3 expression in CD4$^+$ T cells (**d**) and KIR and granzyme B expression in CD8$^+$ T cells (**e**) from WT and KO tonsil cultures 5 days postelectroporation. PBMCs, peripheral blood mononuclear cells; SSC, side scatter. The mean ± s.e.m. is indicated. Significance in **a**–**c** was calculated using a two-sided unpaired *t*-test.

their functions and gauged their effects on self-reactive B and T cells. Ablating the functions of CD4$^+$ T$_{reg}$ cells by knocking out the *FOXP3* gene in tonsillar T cells resulted in production of autoantibodies upon stimulation with a panel of classical autoantigens. This was commensurate with the production of autoantibodies that is a hallmark of *FOXP3* mutations in both humans and mice[12,13], as well as with severe inflammation[14]. Notably, most tonsil organoids exhibited significant increases in the affinity of antigen-specific antibodies, indicating that FOXP3-expressing T cells also suppress generation of high-affinity antibodies. This could explain why most antibody affinities plateau in about the one-nanomolar range[15], perhaps owing to cross-reactivity to self-antigens. To attenuate the function of CD8$^+$ T$_{reg}$ cells, we knocked out the *GZMB* gene, which encodes granzyme B, a critical effector molecule of these cells[16]. This disruption had only a minor effect on autoantibody production but a much more pronounced effect on self-reactive CD8$^+$ and CD4$^+$ T cells. This finding for CD4$^+$ T cells was correlated with the large increase in follicular helper T (T$_{FH}$) cells seen in mice deficient in CD8$^+$ T$_{reg}$ cells[6], a phenotype we also observed in the tonsil organoids. These results suggest that the increase in T$_{FH}$ cells was due to more self-reactive T cells escaping this tolerance checkpoint. Unexpectedly, we found a notable rise in plasmablasts with *GZMB* KO, but this was dependent on T$_{FH}$ cells and was likely to have been an indirect effect. Last, we discovered a significant sex bias in these T$_{reg}$ cell ablations, with tonsils from women typically giving the strongest autoreactive responses. This bias was also observed in unmanipulated tonsillar B cells. This was consistent with the well-known sex biases seen in many autoimmune diseases[17] and could be a useful diagnostic to identify women at risk.

We conclude that CD4$^+$ and CD8$^+$ T$_{reg}$ cells have overlapping yet distinct roles in regulating cellular and humoral responses and preventing autoimmunity. These genetic modifications of the tonsil organoids also demonstrate that we can model key features of how autoreactive B and T cells are controlled and, more broadly, quickly test hypotheses and define mechanisms in a purely human system.

Results

Tonsillar and blood T$_{reg}$ cells differ in frequency and phenotype

CD4$^+$ and CD8$^+$ T$_{reg}$ cells have been characterized in mice and human blood[14,15] but less so in human tonsils. To address this gap, we first investigated and compared the percentages and phenotypes of CD4$^+$ and CD8$^+$ T$_{reg}$ cell subsets in tonsils and peripheral blood cells derived from the same individuals with sleep apnea, with an average age of approximately 40 years. The frequency of FOXP3$^+$CD4$^+$ T$_{reg}$ cells was significantly higher in tonsils compared with blood (Fig. 1a and Extended Data Fig. 1a). Although circulating CD4$^+$ T$_{reg}$ cells usually express high surface levels of CD25 (ref. 18), we found that nearly half of the tonsillar CD4$^+$ T$_{reg}$ cell population expressed low levels of CD25 (ref. 19) (Fig. 1a). In addition, there was a higher percentage of CD4$^+$CXCR5$^+$FOXP3$^+$ follicular T$_{reg}$ cells in the tonsils compared with the blood (Fig. 1b and Extended Data Fig. 1b). The frequencies of CD8$^+$ T$_{reg}$ cells expressing KIR were similar in tonsil and blood samples (Fig. 1c). However, CD8$^+$ T$_{reg}$ cells from the blood displayed significantly higher levels of granzyme B expression (Fig. 1c).

Efficient gene KO using Cas9–RNPs

Next, we aimed to ablate the functional T$_{reg}$ cell subsets to breach self-tolerance in human tonsil organoids[10]. Given that cell depletion using the CD25 surface marker becomes inefficient because more than half of the CD4$^+$ T$_{reg}$ cell population expresses low levels of CD25, we decided to disrupt the suppressive function of the cells by knocking out key genes *FOXP3* and *GZMB* using Cas9 nucleoprotein (RNP). The *FOXP3* gene encodes an important transcription factor that stabilizes

https://doi.org/10.1038/s41590-024-02062-x

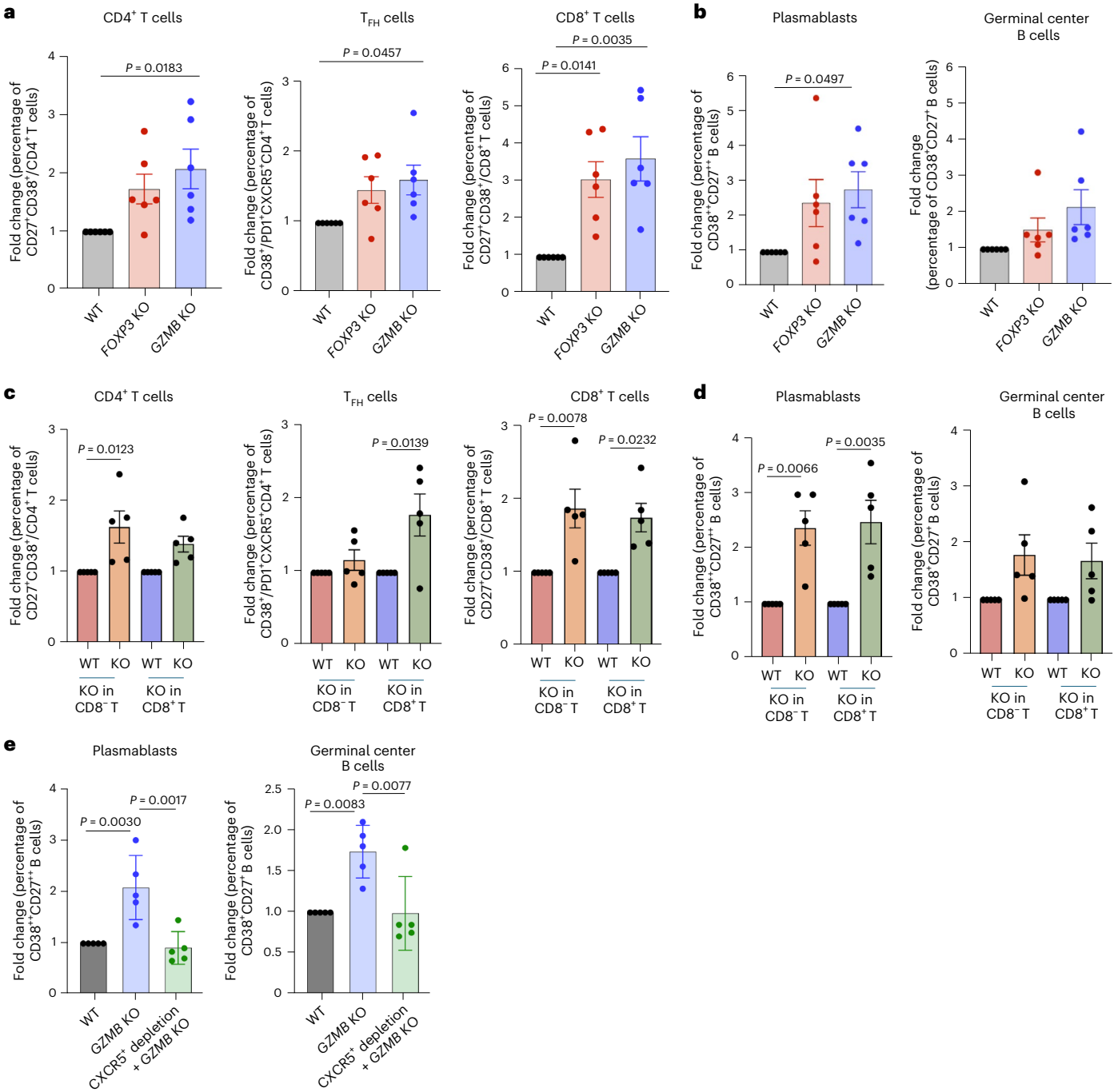

Fig. 2 | Inflammatory T and B cell phenotypes in *FOXP3* and *GZMB* KO tonsil organoids. a,**b**, Statistical analysis of fold change in frequency of activated ($CD27^+CD38^+$) $CD4^+$ and $CD8^+$ T cells and T_{FH} ($CD38^+PD1^+CXCR5^+CD4^+$) cells (**a**) and germinal center B cells and plasmablasts (**b**) in organoids with *FOXP3* KO or *GZMB* KO T cells compared with WT ($n = 6$ donors). **c**,**d**, Statistical analysis of fold change in frequency of activated ($CD27^+CD38^+$) $CD4^+$ and $CD8^+$ T cells and T_{FH} ($CD38^+PD1^+CXCR5^+CD4^+$) cells (**c**) and germinal center B cells ($CD38^+CD27^+$) and plasmablasts ($CD38^{++}CD27^{++}$) (**d**) in organoid culture with *GZMB* KO $CD8^+$ cells or $CD8^-$ T cells compared with WT. **e**, Statistical analysis of fold change in percentage of germinal center B cells and plasmablasts in organoids with WT or *GZMB* KO in $CD8^+$ T cells or in those with $CXCR5^+$ depletion followed by *GZMB* KO in $CD8^+$ T cells compared with WT controls ($n = 5$ donors). Mean ± s.e.m. is indicated. Statistical significance was calculated using one-way analysis of variance (ANOVA) followed by Tukey's multiple comparisons test.

the suppressive function of $CD4^+$ T_{reg} cells[20]. *GZMB* encodes granzyme B, which is essential for the cytotoxic function of $CD8^+$ T cells[21] and has been shown to have high transcript and protein expression levels in activated KIR^+CD8^+ T cells[22]. We isolated total T cells from human tonsils and electroporated them with RNP complexes consisting of the Cas9 protein, *FOXP3*-targeting guide RNAs (gRNAs) or *GZMB*-targeting gRNAs (Extended Data Fig. 1c). gRNAs consisting of scrambled sequences were used as a control to generate wild-type (WT) T cells. To avoid the possibility of the attached beads interfering with the function of antigen-presenting cells (for example, B cells and myeloid cells), we purified the unlabeled CD3-negative cells separately from a new vial of tonsil cells. The CD3-negative cells and electroporated CD3-positive cells were enumerated, combined and plated into transwells at a density of 6×10^6 cells per organoid as before[10]. After 5 days, we assessed the

https://doi.org/10.1038/s41590-024-02062-x

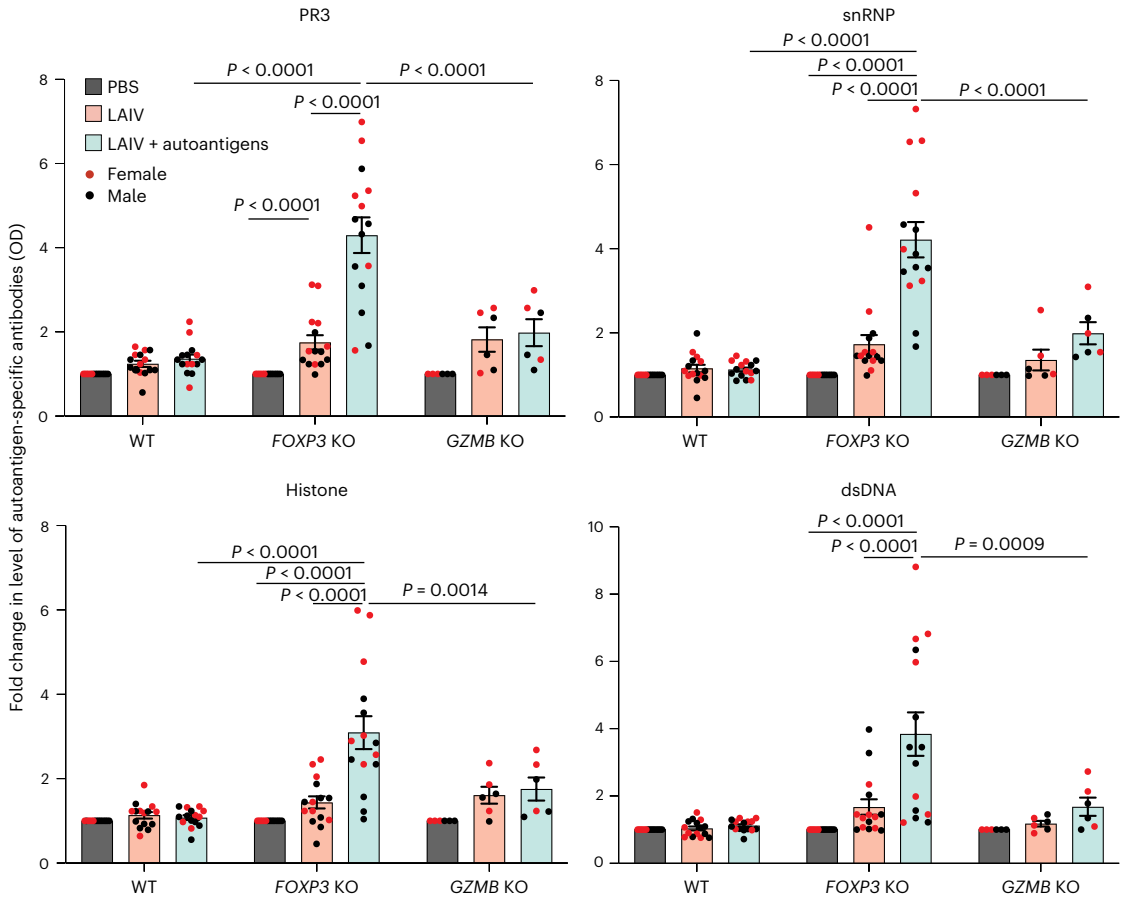

Fig. 3 | Differential autoantigen-specific antibody production in *FOXP3* KO and *GZMB* KO tonsil organoids after stimulation. Autoantibodies specific to PR3, dsDNA, snRNP and core histone were detected in the supernatant of 10-day cultures under the indicated conditions ($n = 15$ for *FOXP3* KO; $n = 6$ donors for *GZMB* KO). The fold change in optical density (OD) values compared with PBS was calculated. The mean ± s.e.m. is indicated. Statistical significance was calculated by two-way ANOVA followed by Tukey's multiple comparisons test.

viability and the KO efficiency by measuring intracellular protein levels via flow cytometry. T cells from WT and KO cultures maintained good viability (90% live cells) (Extended Data Fig. 1d). In *FOXP3* KO tonsil organoids, the intracellular expression of FOXP3 markedly decreased from 14.7% to 0.91% (Fig. 1d). Similarly, in *GZMB* KO cultures, the intracellular expression of granzyme B in KIR^+CD8^+ T cells was significantly reduced, achieving an average KO efficiency of 95% (Fig. 1e). These results demonstrate that highly efficient gene KO can be achieved using Cas9–RNPs in human tonsillar T cells, while maintaining favorable cell viability.

KO tonsil organoids show inflammatory phenotypes

To investigate the impact of ablation of the *FOXP3* and *GZMB* genes in T cells on the overall phenotype of tonsil organoids, we examined the percentages of different B and T cell subsets using surface markers associated with activation and differentiation. In the near absence of *FOXP3* or *GZMB* gene in total T cells, tonsil organoids exhibited signs of inflammation, characterized by increases in percentages of cells expressing activation marker CD38 and costimulation molecule CD27 among both $CD4^+$ and $CD8^+$ T cells compared with WT (Fig. 2a and Extended Data Fig. 2a–d). In addition, there was a significant elevation in the percentage of activated T_{FH} cells from *GZMB* KO tonsil organoids (Fig. 2a and Extended Data Fig. 2e). With both KOs, tonsil organoids showed an increased percentage of germinal center B cells ($CD38^+CD27^+$) and plasmablasts ($CD38^{++}CD27^{++}$) (Fig. 2b and Extended Data Fig. 2f) in most donors.

To further investigate the role of $CD8^+$ T_{reg} cells in the inflammatory phenotypes observed in organoids with *GZMB* KO T cells—particularly given prior reports of cytotoxic effects mediated by $CD4^+$ T_{reg} cells via granzyme B on autoreactive T cells[23]—we replicated experiments by knocking out *GZMB* in either $CD8^+$ or $CD8^-$ T cells (Extended Data Fig. 3a). Our findings revealed significant expansion of $CD4^+$ T cells, T_{FH} cells, $CD8^+$ T cells and plasmablasts within tonsil organoids containing *GZMB* KO $CD8^+$ T cells (Fig. 2c,d and Extended Data Fig. 3b,c). These results were consistent with the phenotypes seen for total T cells. Notably, *GZMB* KO in $CD8^-$ T cells also affected inflammation, as we observed a similar increase in the percentage of the $CD27^+CD38^+$ population, especially in $CD4^+$ T cells, $CD8^+$ T cells and plasmablasts (Fig. 2c,d and Extended Data Fig. 3b,c).

T_{FH} cells play essential parts in the formation of germinal centers and direction of B cell differentiation by providing costimulatory signaling[24–26]. To further investigate whether the expansion of plasmablasts we observed in organoids with *GZMB* KO in $CD8^+$ T cells was due to direct interaction between T and B cells or occurred indirectly via T_{FH} cells, we examined B cell differentiation after efficient depletion of $CXCR5^+$ T cells followed by KO of *GZMB* in $CD8^+$ T cells (Extended Data Fig. 4a,b). When $CXCR5^+$ T cells were depleted, while the number of $CD8^+$ T cells was kept the same as in the WT, there was a significant reduction in the frequency of plasmablasts and germinal center B cells in *GZMB* KO tonsil organoids (Fig. 2e and Extended Data Fig. 4c). This finding suggests that the increased plasmablast levels require the presence of T_{FH} cells and thus are likely to represent an indirect effect.

Differential autoantibody production in KO tonsil organoids

Despite inflammatory phenotypes being observed in B cells within both KO tonsil organoids, there was no significant change in autoantibody

https://doi.org/10.1038/s41590-024-02062-x

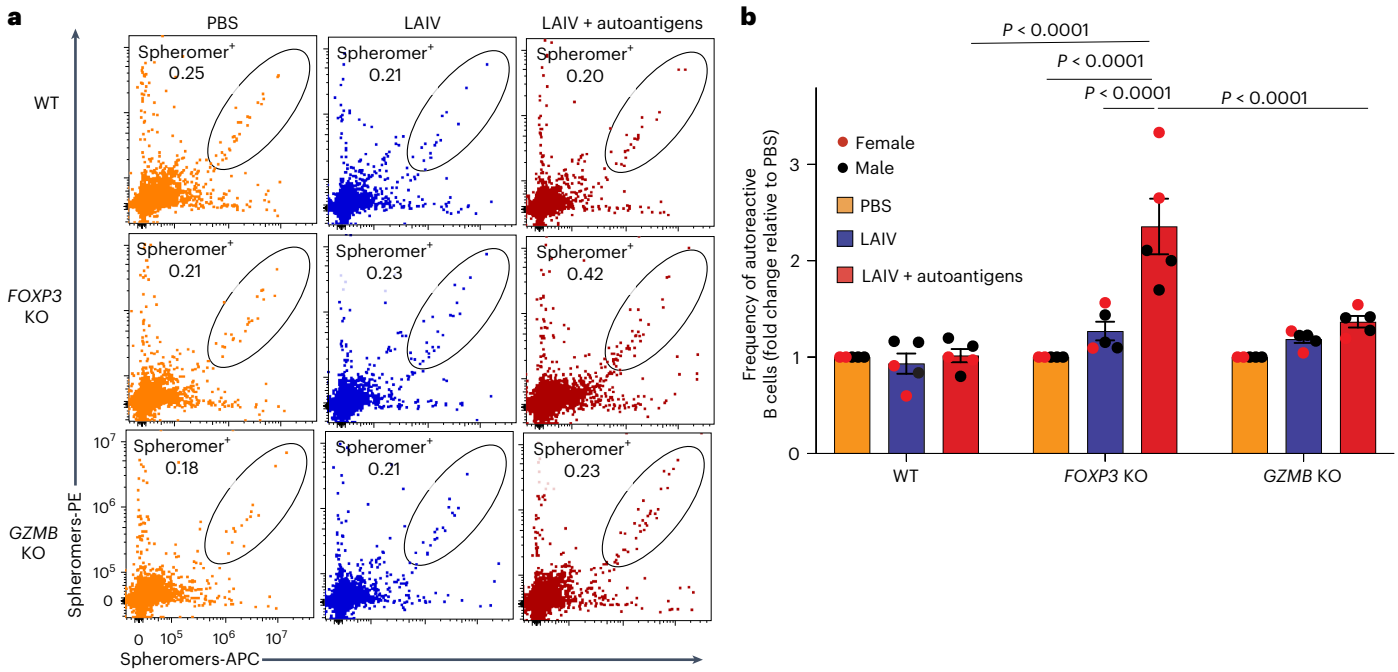

Fig. 4 | Autoreactive B cells expanded from *FOXP3* KO tonsil organoids after stimulation with LAIV and autoantigens. a, Representative FACS plot showing costained spheromer-positive B cells specific to PR3, snRNP-C and core histone (H3.1) after 7 days of culture. **b**, Fold change in the percentage of costained B cells between stimulation and PBS conditions in tonsils with WT, *FOXP3* KO and *GZMB* KO T cells 7 days poststimulation ($n = 5$ donors). The mean ± s.e.m. is indicated. Statistical significance was calculated using two-way ANOVA followed by Tukey's multiple comparisons test.

production compared with WT tonsil organoids, even with addition of the autoantigen to the culture (Extended Data Fig. 5). Previous studies have suggested that viral infection could be a primary factor in initiation of autoimmune diseases[27], and mouse models have shown the development of autoimmune phenotypes following viral infection[6]. Thus, we investigated whether live attenuated influenza vaccine (LAIV) could induce an autoimmune response in the germinal center. The WT, *FOXP3* KO and *GZMB* KO tonsil organoids were stimulated with phosphate-buffered saline (PBS), LAIV alone or a combination of LAIV and autoantigen cocktail. The autoantigen cocktail contained proteinase 3 (PR3), core histones, double-stranded DNA (dsDNA) and small nuclear ribonucleoproteins (snRNP), which are relatively common targets of autoantibodies in patients with autoimmune diseases[28–30] and viral infections[14]. In WT tonsil organoids, LAIV stimulation led to a decreased percentage of $CD4^+$ T_{reg} cells and an increased percentage of $CD8^+$ T_{reg} cells (Extended Data Fig. 6a,b), both characterized by elevated CD38 expression (Extended Data Fig. 6c,d). However, no significant increase in autoantibodies was observed following LAIV stimulation (Fig. 3). By contrast, the *FOXP3*-deficient tonsil organoids showed up to seven-fold higher levels of autoantibodies compared with WT after stimulation with LAIV and autoantigens (Fig. 3). We also observed that most *FOXP3* KO tonsil organoids with high autoantibody production were derived from female donors, whereas stimulated *GZMB* KO tonsil organoids secreted only minimal levels of autoantibodies. These results suggest that $CD4^+$ T_{reg} cells have a more prominent role in control of autoantibody responses compared with $CD8^+$ T_{reg} cells, consistent with *FOXP3* deficiencies observed in mice and humans[10,11].

Autoreactive B cells in *FOXP3* KO organoids expanded after stimulation

The higher levels of autoantibody production in the *FOXP3* KO tonsil organoids led us to hypothesize that the frequency of autoreactive B cells would also be elevated following stimulation. To test this hypothesis, we generated a pool of three 'spheromers', which are highly sensitive multimer reagents based on modified maxi-ferritin[31], specifically targeting the autoantigens PR3, snRNP-C and core histone. In the presence of LAIV, the autoantigen cocktail profoundly stimulated the expansion of self-antigen-specific B cells in *FOXP3* KO tonsil organoids (Fig. 4a,b), consistent with the observed autoantibody levels. Notably, the top two *FOXP3* KO tonsil organoids that produced the higher frequency of autoreactive B cells after LAIV plus autoantigen stimulation were also derived from female donors (Fig. 4b). By contrast, knocking out *GZMB* in tonsillar T cells had only a minor impact on the frequencies of autoreactive B cells (Fig. 4a,b), confirming that $CD4^+$ T_{reg} cells modulate autoantibody secretion by constraining the activation of autoreactive B cells.

Differential autoreactive T cell response in KO organoids

Although *GZMB* KO tonsil organoids generated a mild autoantibody response (Fig. 3), in most donors we observed an increased percentage of activated T cells compared with WT tonsil organoids (Fig. 2a). This suggests that $CD8^+$ T_{reg} cells may exhibit a more robust suppressive response against autoreactive T cell responses. To test this hypothesis, we analyzed the effects of $CD8^+$ T_{reg} cells on $CD8^+$ T cells specific to self-peptides derived from fructose bisphosphate aldolase, keratin, Y-chromosome-encoded SMCY, preproinsulin (PPI) and glutamic acid decarboxylase 65. These self-peptides have previously been detected in the blood of healthy humans, and SMCY-specific $CD8^+$ T cells, in particular, are strictly regulated in males[32]. To detect $CD8^+$ T cells specific to these self-peptides, we generated HLA-A*0201 spheromers and also used a peptide from the hepatitis C virus as a negative control. We stimulated the tonsil organoids with WT, *FOXP3* KO and *GZMB* KO T cells derived from HLA-A*0201 donors with PBS, LAIV, or LAIV supplemented with the autoantigen-derived peptides. After 7 days poststimulation, two of three *FOXP3* KO tonsil organoids showed a two-fold increase in the frequency of self-specific $CD8^+$ T cells. All three *GZMB* KO tonsil organoids showed an almost-three-fold increase with statistical significance in self-peptide-specific $CD8^+$ T cells after stimulation with LAIV and the autoantigen peptide pool (Fig. 5a).

https://doi.org/10.1038/s41590-024-02062-x

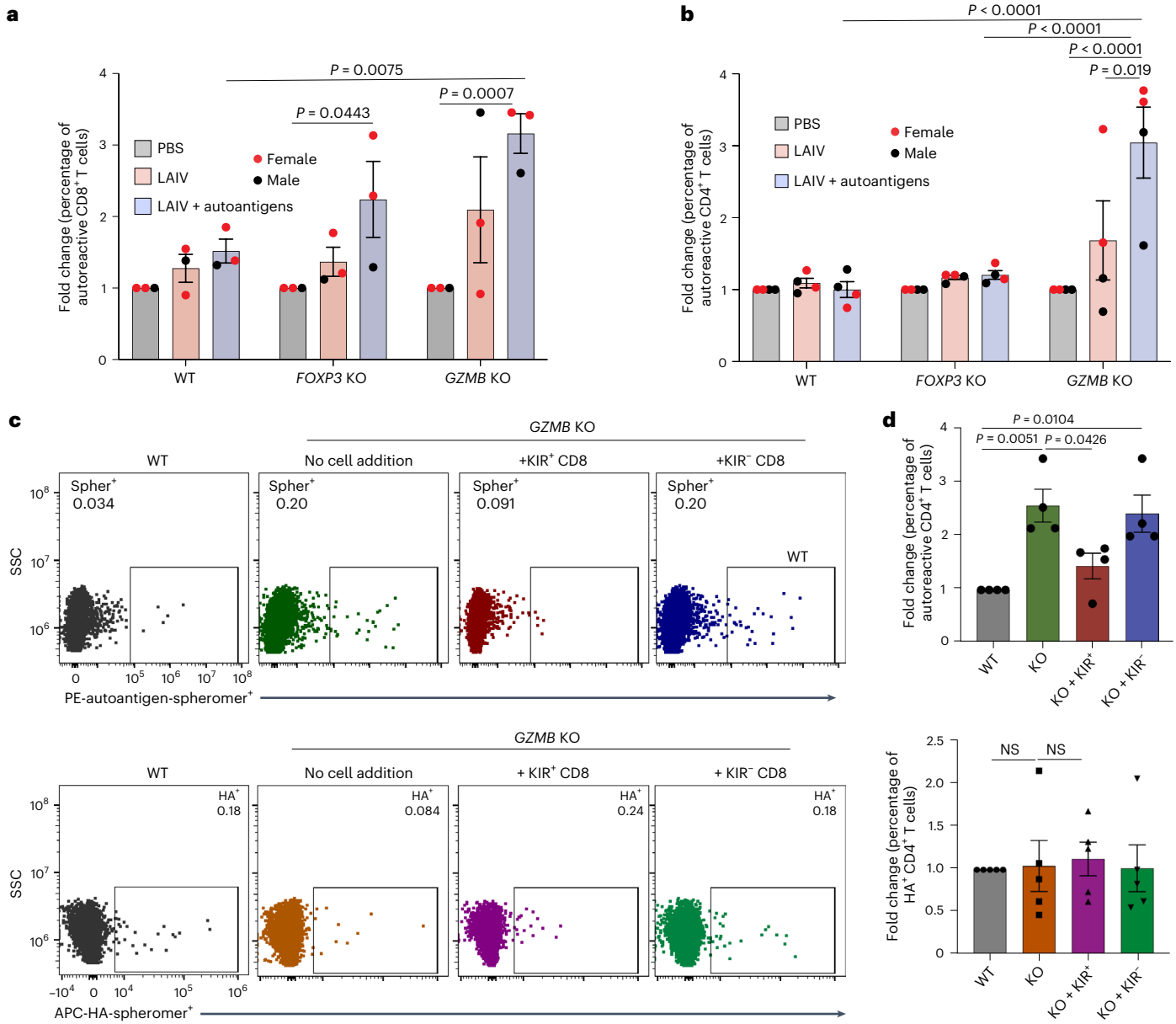

Fig. 5 | Differential CD4⁺ and CD8⁺ T cell responses to autoantigens in *FOXP3* KO and *GZMB* KO tonsil organoids after stimulation with LAIV and autoantigen stimulation. a, HLA-A*0201 tonsil organoids under the indicated WT or KO conditions were cultured for 7 days and then collected for spheromer staining. The percentage of autoreactive CD8⁺ T cells was determined after gating CD8⁺CD3⁺ T cells and human papillomavirus spheromer-negative T cells. The fold change in the percentage of autoreactive T cells under stimulated conditions compared with the control group (treated with PBS) was calculated ($n = 3$ donors). **b**, HLA-DRB1*04:01 tonsil organoids with WT, *FOXP3 KO* or *GZMB* KO total CD3⁺ T cells ($n = 4$ donors) were cultured for 7 days, followed by staining with self-peptide-specific or HA-specific spheromers. The fold change in the percentage of autoreactive-specific CD4⁺ T cells compared with the PBS condition was calculated. **c**, KIR⁺CD8⁺ T cells were depleted, followed by *GZMB* KO in CD8⁺ T cells. Subsequently, KIR⁺CD8⁺ or KIR⁻CD8⁺ T cells were reintroduced into the culture before stimulation with LAIV and autoantigens. Control cultures (WT) received LAIV stimulation without depletion or gene KO. Representative FACS plots show the percentages of spheromer-positive autoreactive CD4⁺ T cells (upper panel) or HA-specific CD4⁺ T cells (lower panel) from tonsil organoids under the indicated conditions. **d**, Fold change in the frequency of autoreactive and HA-specific CD4⁺ T cells compared with WT ($n = 5$ donors). Mean ± s.e.m. is indicated. Statistical significance in **a**, **b** and **d** was calculated using two-way ANOVA followed by Tukey's multiple comparisons test. Spher, spheromer; NS, not significant.

We next investigated the regulation of autoreactive CD4⁺ T cells by T_{reg} cell subsets. We selected self-peptides from gp100, fibrinogen or PPI, as these are relevant in antitumor responses and autoimmunity[33–36]. These antigens can be recognized by CD4⁺ T cells in healthy individuals expressing HLA-DRB1*04:01 (ref. 34). Influenza hemagglutinin (HA)-specific spheromer reagents were included in the staining panel to assess the suppression by CD4⁺ and CD8⁺ T_{reg} cells of autoreactive T cells compared with other activated T cells. Notably, we observed a statistically significant expansion of CD4⁺ T cells specific to self-antigens, particularly in tonsil organoids with *GZMB* KO T cells stimulated by LAIV and autoreactive peptides (Fig. 5b). Whereas HA-reactive CD4⁺ T cells expanded after LAIV stimulation, there was no significant difference in the percentage of HA-specific CD4⁺ T cells across the WT, *FOXP3* KO and *GZMB* KO cultures (Extended Data Fig. 7). Furthermore, the majority of expanded autoreactive CD4⁺ T cells in the *GZMB* KO stimulated tonsil organoids were derived from female donors

https://doi.org/10.1038/s41590-024-02062-x

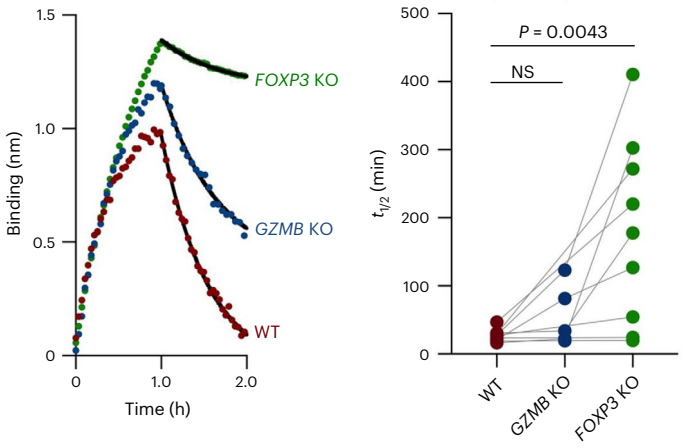

Fig. 6 | *FOXP3* KO enhances antibody affinity, whereas *GZMB* KO shows only a limited effect. Cell supernatants from LAIV-stimulated WT, *GZMB* KO and *FOXP3* KO tonsil cultures were collected after 10 days of culture. Biolayer interferometry assay was performed to measure the binding affinity of antibodies to HA CA/09 hemagglutinin. An overlay of binding traces under the indicated condition is shown. The $t_{1/2}$ was calculated from the off-rates (k_{off}) using the equation for first-order rate kinetics: $t_{1/2} = 0.693/k_{off}$. Statistical significance was determined using one-way ANOVA followed by Tukey's multiple comparisons test. NS, not significant.

(Fig. 5b). By contrast, knocking out *FOXP3* did not affect the frequency of $CD4^+$ T cells specific to self-antigens (Fig. 5b).

To further confirm that the increase in autoreactive $CD4^+$ T cells from *GZMB* KO organoids was specifically due to functional impairment of KIR^+CD8^+ T cells, we depleted KIR^+CD8^+ T cells from tonsils derived from DRB1*04:01$^+$ donors, followed by KO of *GZMB* in $CD8^+$ T cells. KIR^+ and KIR^-CD8^+ T cells were then reintroduced into the culture and supplemented with selected self-peptides from gp100, fibrinogen, or PPI and LAIV cocktail. In the absence of KIR^+CD8^+ T cells and granzyme B, the cocktail profoundly stimulated the expansion of autopeptide-specific $CD4^+$ T cells. Reintroducing KIR^+CD8^+ T cells from the same donor significantly reduced the percentage of autoreactive T cells, whereas introducing an equal amount of KIR^-CD8^+ T cells did not (Fig. 5c,d). By contrast, there was no significant effect on the percentage of HA^+ T cells under comparable conditions. These results suggest that $CD8^+$ T_{reg} cells are a potent suppressor of autoreactive $CD4^+$ T cells.

Overall, our results demonstrate that $CD4^+$ and $CD8^+$ T_{reg} cells have distinct areas of responsibility for suppression of self-reactive lymphocytes, albeit with some overlap.

FOXP3 KO enhances higher antibody affinity

As *FOXP3* is critical in regulation of autoantibody production, we investigated whether it could also affect antibody responses against foreign antigens. Taking advantage of the fact that we had used LAIV as an adjuvant in these experiments, we measured the half-life ($t_{1/2}$) of the elicited antibodies against recombinant influenza hemagglutinin (HA). The tonsil organoids with WT, *FOXP3* KO or *GZMB* KO T cells were stimulated with PBS or LAIV for 10 days. Supernatants from the organoid cultures were collected for the biolayer interferometry assays. Knocking out *FOXP3* in tonsillar T cells led to an increase in the $t_{1/2}$ of the antibodies, such that it was up to 18-fold higher than that in the donor-matched WT condition (Fig. 6), indicating that *FOXP3*-expressing T cells enable production of antibodies with much higher binding affinities in most tonsil donors. The effect of *GZMB* KO was less dramatic, with an average two-fold improvement in five donors. These data indicate that $CD4^+$ T_{reg} cells not only regulate autoreactive B cells but also have an impact on B cells in general, effectively limiting their affinity to the typical range, at or near 1 nM.

Higher autoreactivity in organoids from women compared with men

In recent years, risk factors associated with autoimmune diseases, such as sex and aging, have garnered significant attention[37,38]. Using our tonsil organoid system, we explored some factors that might be associated with self-reactive antibodies. A previous study showed that early immature B cells in healthy donors could produce self-reactive antibodies[39]. Thus, we investigated whether autoreactive B cells were also present in tonsils and whether there was a correlation with sex. For this purpose, we used biotinylated spheromers specific to PR3, snRNP or core histone, coupled with PE- or APC-conjugated streptavidin, and costained tonsil samples from age-matched male and female donors. In most donors, we successfully detected B cells specific to these autoantigens, constituting approximately 0.01% to 0.2% of B cells. Notably, these higher levels were found only in the female donors (Fig. 7a,b). Next, we investigated whether sex and chronological age contributed to the autoantibody production we observed in stimulated tonsil organoids with *FOXP3* KO T cells. Indeed, we found a strong correlation between autoantibody production and age, with higher levels of autoantibodies detected in donors above 40 years of age (Fig. 7c). These results highlight the unique and representative nature of tonsil cells and organoids as a valuable system for hypothesis testing and mechanistic studies related to human autoimmune diseases.

Discussion

Although we have learned a great deal about the characteristics and importance of *FOXP3*-expressing $CD4^+$ T cells in enforcing self-tolerance[40–44], it has only recently emerged that a small subset of $CD8^+$ T cells, characterized by Ly49 expression in mice and KIR expression in humans, also plays an important part[7–9]. These $CD8^+$ T_{reg} cells are particularly active in the intestines during acute celiac disease and are elevated in patients with other autoimmune diseases, as well as during infections in humans and mice[8]. Conditional KO of the predominant *Ly49* gene in mice leads to autoimmune sequelae following either influenza or lymphocytic choriomeningitis virus infection[8]. The importance of both T_{reg} cell types in controlling self-reactivity raises the question of what their specific roles might be. To address this question, we made use of our recent demonstration that a type of organoid made from human tonsil cells could reproduce many of the hallmarks of an adaptive immune response in vitro, especially when stimulated with various vaccines[10,11]. The single-cell suspensions of tonsil cells as a starting point for organoid culture provide an ideal platform for using CRISPR–Cas9 gene editing to disable $CD4^+$ and $CD8^+$ T_{reg} cells to analyze their relative roles in controlling autoreactive T and B cells.

Knocking out *FOXP3* resulted in expansion of self-reactive B cells and production of autoantibodies. Autoantibodies are a characteristic of *FOXP3* disruption in humans and mice[45,46]; thus, this effect in the tonsil organoids phenocopies the in vivo results. However, it was surprising that despite both *FOXP3* and *GZMB* KO resulting in similar levels of T_{FH} cells and plasma cells, the latter had only a minimal impact on autoantigen-specific antibody production. Given that $CD8^+KIR^+$ T_{reg} cells are known to target T_{FH} cells, as observed in our study and others[7,47], but do not affect antibody production, we speculate that the effects of $CD4^+$ T_{reg} cells on autoantibody production are exerted through direct interaction with B cells. This is supported by previous work showing that $CD4^+$ T_{reg} cells are present in follicles and T–B borders in human tonsils and can directly suppress B cell class switch recombination[48], as well as inhibiting autoantibody-producing B cells in vitro[49]. Although *FOXP3* ablation in human T_{reg} cells does not affect CD25 and CTLA-4 expression[50], other signaling molecules may be involved, considering the potential impact of FOXP3 on genome architectural functions and transcriptional regulation[51]. Given the diverse $FOXP3^+$ T_{reg} cell population[52], understanding which subsets contribute to autoantibody production and B cell regulation is crucial.

https://doi.org/10.1038/s41590-024-02062-x

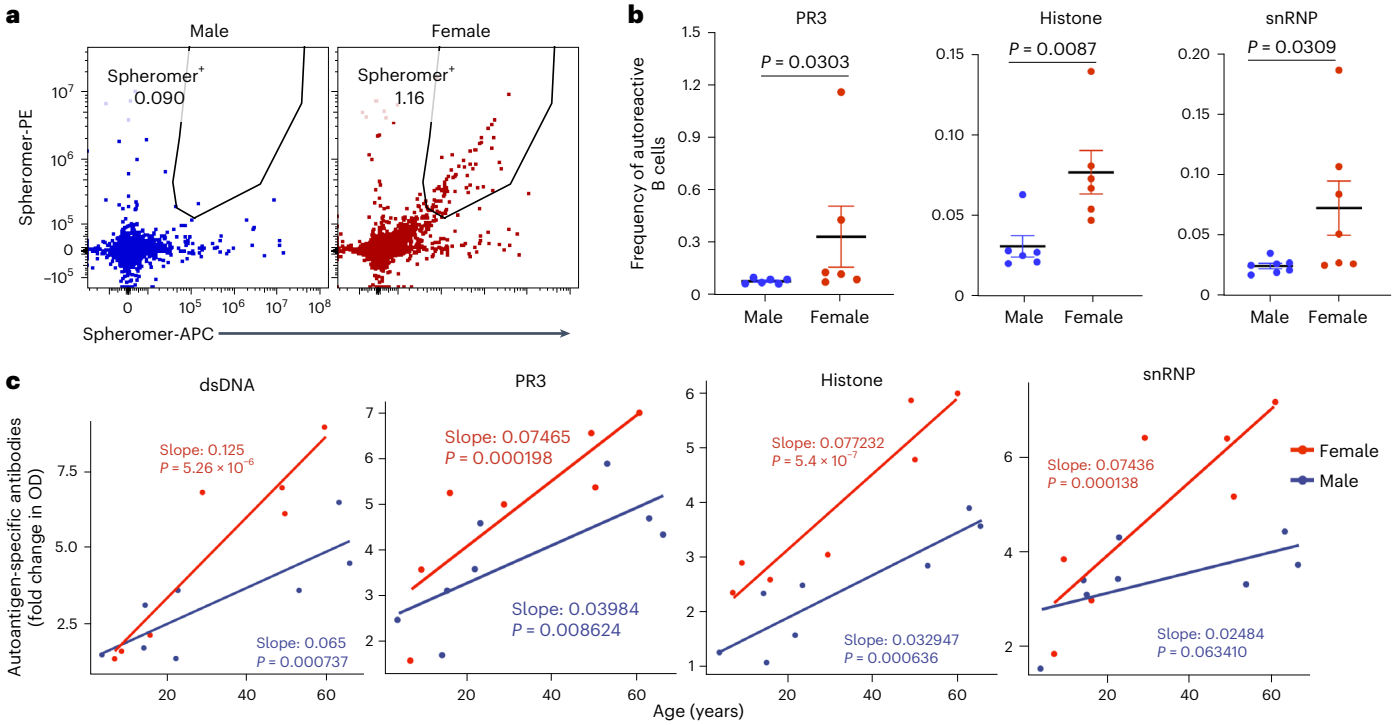

Fig. 7 | Tonsillar B cells show a higher frequency of autoreactivity in women versus men, regardless of attenuating T_{reg} cells. a, Representative FACS plots showing spheromer (PR3)-positive tonsillar B cells from age-matched male and female donors. **b**, Dot plots illustrating the percentage of B cells specific to PR3, histone and snRNP from age-matched donors ($n = 6$). **c**, Autoantibodies specific to PR3, dsDNA, snRNP and core histone were detected by ELISA in the supernatant of 10-day cultures from organoids with WT and *FOXP3* KO T cells ($n = 15$) stimulated with LAIV and autoantigen pools. The fold change in optical density compared with PBS was analyzed using a linear regression model to predict the correlations between autoantibody levels, age and sex. The regression model coefficients (slopes) represent the effect of age on the response variable for each sex, with *P* values indicating statistical significance. Model statistics (*F*-statistic, *P* value and adjusted R^2) are reported for each autoantibody: dsDNA: $F(2,12) = 30.08$, $P = 2.115 \times 10^{-5}$, adjusted $R^2 = 0.806$; PR3: $F(2,12) = 13.97$, $P = 0.0007357$, adjusted $R^2 = 0.649$; histone: $F(2,12) = 46.49$, $P = 2.231 \times 10^{-6}$, adjusted $R^2 = 0.8666$; snRNP: $F(2,12) = 15.58$, $P = 0.0004622$, adjusted $R^2 = 0.6756$. In **b**, significance was calculated using one-sided Mann–Whitney test; mean ± s.e.m. is indicated.

We also observed substantial increases in the bulk serological affinity of influenza-specific antibodies in most of the *FOXP3*-deficient organoids and to a lesser extent in *GZMB* KOs; this is reminiscent of the increased affinity for self-specific antibodies in *AIRE*-deficient individuals[53,54] and indicates that disrupting T cell tolerance allows the emergence of higher-affinity antibodies. This is likely to relate to the phenomenon by which the higher the affinity of an antibody, the greater the chances of pathological cross-reactivity to one or more self-antigens[55,56]. This result also suggests a reason that most monoclonal antibodies typically fall within the low nanomolar range and rarely higher[54].

Our results highlight the differential roles of $CD4^+$ and $CD8^+$ T_{reg} cells in regulating autoimmunity, potentially by targeting different cellular activities and involvement in different stages of autoimmune development. *GZMB* KO allowed both autoreactive $CD4^+$ and $CD8^+$ T cells to proliferate, demonstrating that $CD8^+$ T_{reg} cells are the major factor controlling T cell tolerance, especially for autoreactive $CD4^+$ T cells. This $CD4^+$ effect was earlier observed by the marked increase in T_{FH} cells in mice deficient in $CD8^+$ T_{reg} cells[6,8], suggesting that more T_{FH} cells were allowed to expand than normal when $CD8^+$ T_{reg} cell activity was absent or attenuated. In addition, previous work with patients infected with SARS-CoV-2 or influenza has demonstrated increased proportions of $CD8^+$ T_{reg} cells during these infections but no change in $CD4^+$ T_{reg} cells[8,9]. Infection is a crucial trigger for the breakdown of tolerance, with many autoimmunity patients reporting an infection just before the onset of clinical symptoms[57]. Thus, the disruption of $CD8^+$ T_{reg} cell control could be a key first step in triggering clinical autoimmunity. However, as autoantibodies can precede autoimmune disease by years[58–61], there is likely to be a loss of $CD4^+$ T_{reg} cell control earlier.

In summary, we have developed human tonsil organoid models of autoimmunity using CRISPR–Cas9 gene editing techniques. By performing targeted KO, we investigated the distinct roles of two different T_{reg} cell subsets. Knocking out *FOXP3* in the $CD4^+$ T_{reg} cell within the tonsil organoids resulted in a drastic increase in autoreactive B cells, autoantibodies and antigen-specific antibody affinity. On the other hand, knocking out *GZMB* in T cells led to dysfunction of $CD8^+$ T_{reg} cells, promoting the expansion of T_{FH} cells and autoreactive $CD4^+$ and $CD8^+$ T cells, and enhancing B cell differentiation. These findings align with observations made in mouse models and patients with defective $CD4^+$ and $CD8^+$ T_{reg} cells. Further exploration of the tonsil organoid model holds significant potential for identifying new mechanisms and translating them into therapeutic approaches for autoimmune diseases.

Online content

Any methods, additional references, Nature Portfolio reporting summaries, source data, extended data, supplementary information, acknowledgements, peer review information; details of author contributions and competing interests; and statements of data and code availability are available at https://doi.org/10.1038/s41590-024-02062-x.

References

1. Valent, P. et al. Paul Ehrlich (1854-1915) and his contributions to the foundation and birth of translational medicine. *J. Innate Immun.* **8**, 111–120 (2016).
2. Goodnow, C. C. et al. Altered immunoglobulin expression and functional silencing of self-reactive B lymphocytes in transgenic mice. *Nature* **334**, 676–682 (1988).

3. Asano, M., Toda, M., Sakaguchi, N. & Sakaguchi, S. Autoimmune disease as a consequence of developmental abnormality of a T cell subpopulation. *J. Exp. Med.* **184**, 387–396 (1996).
4. Baecher-Allan, C. & Hafler, D. A. Human regulatory T cells and their role in autoimmune disease. *Immunol. Rev.* **212**, 203–216 (2006).
5. Jiang, H., Zhang, S. I. & Pernis, B. Role of CD8+ T cells in murine experimental allergic encephalomyelitis. *Science* **256**, 1213–1215 (1992).
6. Kim, H. J. et al. Stable inhibitory activity of regulatory T cells requires the transcription factor Helios. *Science* **350**, 334–339 (2015).
7. Kim, H. J., Verbinnen, B., Tang, X., Lu, L. & Cantor, H. Inhibition of follicular T-helper cells by $CD8^+$ regulatory T cells is essential for self tolerance. *Nature* **467**, 328–332 (2010).
8. Li, J. et al. KIR^+CD8^+ T cells suppress pathogenic T cells and are active in autoimmune diseases and COVID-19. *Science* **376**, eabi9591 (2022).
9. Saligrama, N. et al. Opposing T cell responses in experimental autoimmune encephalomyelitis. *Nature* **572**, 481–487 (2019).
10. Wagar, L. E. et al. Modeling human adaptive immune responses with tonsil organoids. *Nat. Med.* **27**, 125–135 (2021).
11. Kastenschmidt, J. M. et al. Influenza vaccine format mediates distinct cellular and antibody responses in human immune organoids. *Immunity* **56**, 1910–1926.e7 (2023).
12. Hadaschik, E. N. et al. Regulatory T cell-deficient scurfy mice develop systemic autoimmune features resembling lupus-like disease. *Arthritis Res. Ther.* **17**, 35 (2015).
13. Tsuda, M. et al. The spectrum of autoantibodies in IPEX syndrome is broad and includes anti-mitochondrial autoantibodies. *J. Autoimmun.* **35**, 265–268 (2010).
14. Chang, S. E. et al. New-onset IgG autoantibodies in hospitalized patients with COVID-19. *Nat. Commun.* **12**, 5417 (2021).
15. Poulsen, T. R., Jensen, A., Haurum, J. S. & Andersen, P. S. Limits for antibody affinity maturation and repertoire diversification in hypervaccinated humans. *J. Immunol.* **187**, 4229–4235 (2011).
16. Choi, S. J. et al. KIR^+CD8^+ and $NKG2A^+CD8^+$ T cells are distinct innate-like populations in humans. *Cell Rep.* **42**, 112236 (2023).
17. Rubtsova, K., Marrack, P. & Rubtsov, A. V. Sexual dimorphism in autoimmunity. *J. Clin. Invest.* **125**, 2187–2193 (2015).
18. Dieckmann, D., Plottner, H., Berchtold, S., Berger, T. & Schuler, G. Ex vivo isolation and characterization of $CD4^+CD25^+$ T cells with regulatory properties from human blood. *J. Exp. Med.* **193**, 1303–1310 (2001).
19. Baecher-Allan, C. M. & Hafler, D. A. The purification and functional analysis of human $CD4^+CD25^{high}$ regulatory T cells. *Curr. Protoc. Immunol.* **72**, 7.4B.1–7.4B.12 (2006).
20. Hori, S., Nomura, T. & Sakaguchi, S. Control of regulatory T cell development by the transcription factor Foxp3. *Science* https://doi.org/10.1126/science.1079490 (2003).
21. Salti, S. M. et al. Granzyme B regulates antiviral CD8+ T cell responses. *J. Immunol.* **187**, 6301–6309 (2011).
22. Li, J. et al. KIR^+CD8^+ T cells suppress pathogenic T cells and are active in autoimmune diseases and COVID-19. *Science* https://doi.org/10.1126/science.abi9591 (2022).
23. Loebbermann, J. et al. Regulatory T cells expressing granzyme B play a critical role in controlling lung inflammation during acute viral infection. *Mucosal Immunol.* **5**, 161–172 (2012).
24. Ise, W. et al. T follicular helper cell-germinal center B cell interaction strength regulates entry into plasma cell or recycling germinal center cell fate. *Immunity* **48**, 702–715.e4 (2018).
25. Mintz, M. A. & Cyster, J. G. T follicular helper cells in germinal center B cell selection and lymphomagenesis. *Immunol. Rev.* **296**, 48–61 (2020).
26. Shulman, Z. et al. T follicular helper cell dynamics in germinal centers. *Science* **341**, 673–677 (2013).
27. Getts, D. R., Chastain, E. M., Terry, R. L. & Miller, S. D. Virus infection, antiviral immunity, and autoimmunity. *Immunol. Rev.* **255**, 197–209 (2013).
28. Dieker, J. et al. Autoantibodies against modified histone peptides in SLE patients are associated with disease activity and lupus nephritis. *PLoS ONE* **11**, e0165373 (2016).
29. Kattah, N. H., Kattah, M. G. & Utz, P. J. The U1-snRNP complex: structural properties relating to autoimmune pathogenesis in rheumatic diseases. *Immunol. Rev.* **233**, 126–145 (2010).
30. Primo, V. C. et al. Anti-PR3 immune responses induce segmental and necrotizing glomerulonephritis. *Clin. Exp. Immunol.* **159**, 327–337 (2010).
31. Mallajosyula, V. et al. $CD8^+$ T cells specific for conserved coronavirus epitopes correlate with milder disease in patients with COVID-19. *Sci. Immunol.* https://doi.org/10.1126/sciimmunol.abg5669 (2021).
32. Yu, W. et al. Clonal deletion prunes but does not eliminate self-specific αβ $CD8^+$ T lymphocytes. *Immunity* **42**, 929–941 (2015).
33. Nielen, M. M. et al. Antibodies to citrullinated human fibrinogen (ACF) have diagnostic and prognostic value in early arthritis. *Ann. Rheum. Dis.* **64**, 1199–1204 (2005).
34. Su, L. F., Kidd, B. A., Han, A., Kotzin, J. J. & Davis, M. M. Virus-specific $CD4^+$ memory-phenotype T cells are abundant in unexposed adults. *Immunity* **38**, 373–383 (2013).
35. Yuan, J. et al. Safety and immunogenicity of a human and mouse gp100 DNA vaccine in a phase I trial of patients with melanoma. *Cancer Immun.* **9**, 5 (2009).
36. Zhang, L., Nakayama, M. & Eisenbarth, G. S. Insulin as an autoantigen in NOD/human diabetes. *Curr. Opin. Immunol.* **20**, 111–118 (2008).
37. Goronzy, J. J. & Weyand, C. M. Immune aging and autoimmunity. *Cell. Mol. Life Sci.* **69**, 1615–1623 (2012).
38. Whitacre, C. C. Sex differences in autoimmune disease. *Nat. Immunol.* **2**, 777–780 (2001).
39. Wardemann, H. et al. Predominant autoantibody production by early human B cell precursors. *Science* https://doi.org/10.1126/science.1086907 (2003).
40. Fontenot, J. D., Gavin, M. A. & Rudensky, A. Y. Foxp3 programs the development and function of $CD4^+CD25^+$ regulatory T cells. *Nat. Immunol.* **4**, 330–336 (2003).
41. Kim, J. M. & Rudensky, A. The role of the transcription factor Foxp3 in the development of regulatory T cells. *Immunol. Rev.* **212**, 86–98 (2006).
42. Sakaguchi, S. Naturally arising Foxp3-expressing $CD25^+CD4^+$ regulatory T cells in immunological tolerance to self and non-self. *Nat. Immunol.* **6**, 345–352 (2005).
43. Yang, S., Fujikado, N., Kolodin, D., Benoist, C. & Mathis, D. Immune tolerance. Regulatory T cells generated early in life play a distinct role in maintaining self-tolerance. *Science* **348**, 589–594 (2015).
44. Zheng, Y. & Rudensky, A. Y. Foxp3 in control of the regulatory T cell lineage. *Nat. Immunol.* **8**, 457–462 (2007).
45. Hoshino, A. et al. Identification of autoantibodies using human proteome microarrays in patients with IPEX syndrome. *Clin. Immunol.* **203**, 9–13 (2019).
46. Kinnunen, T. et al. Accumulation of peripheral autoreactive B cells in the absence of functional human regulatory T cells. *Blood* **121**, 1595–1603 (2013).
47. McCarron, M. J. & Marie, J. C. TGF-beta prevents T follicular helper cell accumulation and B cell autoreactivity. *J. Clin. Invest.* **124**, 4375–4386 (2014).
48. Lim, H. W., Hillsamer, P., Banham, A. H. & Kim, C. H. Cutting edge: direct suppression of B cells by $CD4^+CD25^+$ regulatory T cells. *J. Immunol.* https://doi.org/10.4049/jimmunol.175.7.4180 (2005).
49. Iikuni, N., Lourenço, E. V., Hahn, B. H. & La, C. Cutting edge: regulatory T cells directly suppress B cells in systemic lupus erythematosus. *J. Immunol.* https://doi.org/10.4049/jimmunol.0901163 (2009).

50. Lam, A. J. et al. Optimized CRISPR-mediated gene knockin reveals FOXP3-independent maintenance of human Treg identity. *Cell Rep.* **36**, 109494 (2021).
51. Zhang, W. et al. FOXP3 recognizes microsatellites and bridges DNA through multimerization. *Nature* **624**, 433–441 (2023).
52. Le Coz, C. et al. Human T follicular helper clones seed the germinal center-resident regulatory pool. *Sci. Immunol.* **8**, eade8162 (2023).
53. Davis, M. M. In praise of descriptive science: a breath of fresh AIRE. *Cell* **166**, 530–531 (2016).
54. Meyer, S. et al. AIRE-deficient patients harbor unique high-affinity disease-ameliorating autoantibodies. *Cell* **166**, 582–595 (2016).
55. Rabia, L. A., Desai, A. A., Jhajj, H. S. & Tessier, P. M. Understanding and overcoming trade-offs between antibody affinity, specificity, stability and solubility. *Biochem. Eng. J.* **137**, 365–374 (2018).
56. Suurmond, J. & Diamond, B. Autoantibodies in systemic autoimmune diseases: specificity and pathogenicity. *J. Clin. Invest.* **125**, 2194–2202 (2015).
57. Sundaresan, B., Shirafkan, F., Ripperger, K. & Rattay, K. The role of viral infections in the onset of autoimmune diseases. *Viruses* https://doi.org/10.3390/v15030782 (2023).
58. Arbuckle, M. R. et al. Development of anti-dsDNA autoantibodies prior to clinical diagnosis of systemic lupus erythematosus. *Scand. J. Immunol.* **54**, 211–219 (2001).
59. Arbuckle, M. R. et al. Development of autoantibodies before the clinical onset of systemic lupus erythematosus. *N. Engl. J. Med.* **349**, 1526–1533 (2003).
60. Leslie, D., Lipsky, P. & Notkins, A. L. Autoantibodies as predictors of disease. *J. Clin. Invest.* **108**, 1417–1422 (2001).
61. Olsen, N. J., Okuda, D. T., Holers, V. M. & Karp, D. R. Editorial: understanding the concept of pre-clinical autoimmunity. *Front. Immunol.* **13**, 983310 (2022).

Methods

Human samples and tonsil processing

The collection and processing of tonsil samples from children and adult volunteers were covered by institutional review board (IRB) protocols 30837 and 60741, approved by the Stanford University IRB. Blood from healthy donors was requested from the Stanford Blood Center under IRB protocol 40146. Written informed consent was obtained from adult participants and from the legal guardians of children aged 0–17 years. No participant compensation was provided for the participants. Any individuals who were taking systemic immunomodulatory drugs, had a history of immunosuppressive or autoimmune diseases, or had a serious active infection at the time of the procedure were excluded.

The procedures for tonsil samples followed those described in a previous study[10]. Tonsil samples were collected immediately after surgery and incubated in Ham's F-12 medium (Gibco) containing Normocin (InvivoGen), penicillin and streptomycin for at least 1 h at 4 °C before processing. Afterward, tonsil tissue was manually sectioned into small pieces (~5 mm × 5 mm × 5 mm) and passed through a 100-mM filter using a syringe plunger to obtain a cell suspension. The filter was repeatedly washed with complete medium to help filter the cells. Complete medium included RPMI supplemented with Glutamax (Thermo Fisher), 10% fetal bovine serum (FBS), 1× penicillin–streptomycin, 1× Normocin (InvivoGen), 1× insulin–transferrin–selenium supplement (Gibco), 1× nonessential amino acids and 1× sodium pyruvate. Debris was reduced by Ficoll density gradient separation. Collected cells were washed with PBS, enumerated and frozen into cryovials in FBS + 10% dimethyl sulfoxide. Frozen aliquots were stored at −140 °C until use.

Blood processing

Blood was diluted with cell culture medium and 2% FBS in a 1:1 volume ratio. This diluted blood was then carefully placed on top of a density gradient medium (Ficoll-Paque, GE Healthcare) and centrifuged at 800*g* for 20 min without the brake. For collection of peripheral blood mononuclear cells, a pipette was inserted directly through the upper plasma layer into the interface containing the mononuclear cells. The collected cells were washed twice with medium, frozen in aliquots using FBS with 10% dimethyl sulfoxide and stored at −140 °C until needed.

Cas9–RNP assembly and electroporation

Cas9–RNPs (Integrated DNA Technologies) were prepared by incubating 20 µM Cas9 with 20 µM gRNA (Synthego) at a 1:1 ratio at 37 °C for 15 min, resulting in a final concentration of 10 µM. The sequences of oligonucleotides are provided in Supplementary Table 1. Electroporation was performed using reagents from a P3 Primary Cell 4D-Nucleofector X Kit S (Lonza) according to the manufacturer's instructions. Target T cells were gently suspended in P3 buffer supplemented with supplement 1 reagent at a density of 10–20 million cells per 20 µl. The Cas9–RNPs and T cells were mixed gently in the P3 buffer. This mixture was then transferred to a 4D-Nucleofector cuvette from Lonza Bioscience and subjected to electroporation using code EH105. Following electroporation, the cuvette was placed in the tissue culture incubator at 37 °C for 30 min to allow the cells to recover. Once recovered, the cells were ready to be cultured in transwells.

Cell sorting and organoid assembly

For KO experiments involving total T cells, T cells were isolated from tonsil single-cell suspensions using a Human Pan T Cell Isolation Kit (Miltenyi Biotec) for electroporation. $CD3^-$ cells were obtained by depleting $CD3^+$ T cells using CD3 MicroBeads, human (Miltenyi Biotec). Organoids were reassembled by combining KO $CD3^+$ T cells with $CD3^-$ cells at the same donor-specific cell ratio and cultured at a density of 6×10^6 cells in 100 µl per transwell.

For *GZMB* KO experiments in $CD8^+$ T cells, untouched $CD8^+$ T cells were isolated using a $CD8^+$ T Cell Isolation Kit, human (Miltenyi Biotec) for electroporation. The $CD8^-$ cell fraction was collected by staining the tonsil single-cell suspension with CD8-PE antibody for 30 min at 4 °C, followed by depletion with anti-PE MicroBeads (Miltenyi Biotec). KO organoids were reassembled by combining $CD8^+$ T cells with $CD8^-$ cells at the same donor-specific cell ratio and cultured in transwells.

For *GZMB* KO experiments in $CD8^-$ T cells, untouched $CD3^+$ T cells were first isolated using a Pan T Cell Isolation Kit, human (Miltenyi Biotec), followed by $CD8^+$ T cell depletion using a REAlease CD8 MicroBead Kit, human (Miltenyi Biotec). After electroporation and a 30-min recovery, the $CD3^-$ cells, $CD8^+$ T cells (beads removed according to the manufacturer's instructions) and *GZMB* KO $CD8^-$ T cells were recombined at the same donor-specific cell ratio and cultured at 6×10^6 cells in 100 µl per transwell.

For CXCR5 depletion followed by *GZMB* KO in $CD8^+$ T cells, tonsil single-cell suspensions were stained with anti-human CD8-PE (BioLegend) and CXCR5-PE (BioLegend) antibodies at room temperature in the dark for 30 min. PE-positive cells were depleted using anti-PE MicroBeads (Miltenyi Biotec) according to the manufacturer's instructions. Untouched $CD8^+$ T cells were isolated using a $CD8^+$ T Cell Isolation Kit, human (Miltenyi Biotec), followed by electroporation. Finally, the KO $CD8^+$ T cells were combined with the $CD8^-CXCR5^-$ cell population at the same donor-specific cell ratio.

Cell culture and stimulation

For culture of cryopreserved cells, aliquots were thawed into complete medium, enumerated and resuspended to 6×10^7 cells per ml for larger cultures or 2×10^7 cells per ml for smaller cultures. Then, 6×10^6 cells in 100 µl were plated into each 12-mm cell culture insert, which had a 0.4-µm pore size (Millipore Sigma). 1 ml complete medium supplemented with 1 ng ml^{-1} IL-21 was added to the lower chamber. 1 µl LAIV (Intranasal FluMist Quadrivalent 2022–2023) was added per well, equivalent to 1.6×10^4 to 1.6×10^5 fluorescent focus units per strain. 1 µg ml^{-1} autoantigens were added in some experiments. 1 µg ml^{-1} of recombinant human B cell-activating factor (BioLegend) may be added to the culture after 4 days. Cell cultures were incubated at 37 °C, 5% CO_2 with humidity, and supplemented with additional medium to the lower wells as necessary.

$CD8^+KIR^+$ functional assay

$CD8^+$ T cells were purified from tonsil cells using CD8 microbeads (Miltenyi Biotec) per the manufacturer's instructions and stained with flow antibodies, and live $CD8^+KIR^+$ or $CD8^+KIR^-$ T cells were sorted out by flow cytometry (BD). Sorted KIR^-CD8^+ T cells were added back to $CD8^-$ tonsil cells, mixed with Cas9 protein and *GZMB* gRNA or scrambled gRNA (as WT) to perform KO. After being allowed to rest for 30 min postelectroporation, equal numbers of KIR^+ or KIR^-CD8^+ T cells were added to the culture of KIR^- tonsil cells at a 1:50 ratio. A total of 6×10^6 cells per condition in 100 µl were plated into each 12-mm cell culture insert, which had a 0.4-µm pore size (Millipore Sigma). Then, 1 ml complete medium supplemented with 1 µl LAIV (Intranasal FluMist Quadrivalent 2022–2023, equivalent to 1.6×10^4 to 1.6×10^5 fluorescent focus units per strain) and 10 µg ml^{-1} autopeptides was added to the lower chamber. After day 4, 300 U ml^{-1} of IL-2 and 1 µg ml^{-1} of recombinant human B cell-activating factor (BioLegend) were added to the culture. Cell cultures were incubated at 37 °C, 5% CO_2 with humidity, and supplemented with additional medium to the lower wells as necessary.

Flow cytometry

Culture organoids were resuspended by rinsing the membrane with medium and collected from the transwells. Cells were washed with fluorescence-activated cell sorting (FACS) buffer (PBS + 0.1% bovine serum albumin, 0.05% sodium azide and 2 mM EDTA) and treated with Fc receptor block (BioLegend, 10 µg ml^{-1}) in FACS buffer for 10 min,

followed by staining with live/dead Aqua Zombie stain (Thermo Fisher) and antibodies against surface markers (30 min, 4 °C). Antibodies against surface markers include anti-human CD3 (BUV805, Clone UCHT1, BD) and anti-human CD19 (BUV737, Clone HIB19, BD), anti-human CD4 (BV650, Clone OKT4, BioLegend), anti-human CD8 (BV421, Clone BPA-T8, BioLegend), anti-human CXCR5 (PE-Dazzle 594, Clone J252D4, BioLegend), anti-human PD1 (APC, Clone EH12.2H7, BioLegend), anti-human CD38 (Alexa Fluor 700, Clone HIT2, BioLegend), anti-human CD27 (Pecy7, Clone 0323, BioLegend), anti-human KIR3DL1 (PE, Clone DX9, BioLegend), anti-human KIR2DL2/L3/S2 (PE, Clone DX27, BioLegend), anti-human KIR2DL5 (PE, Clone UP-R1, BioLegend), anti-human CD25 (BV711, Clone M-A251, BioLegend) and anti-human KIR2DL2/L3 (PE, DX27, BioLegend). For intracellular staining, the cells were fixed and permeabilized with the Intracellular Fixation & Permeabilization Buffer Set (eBioscience) followed by staining with anti-human FOXP3 (AF647 or AF488, Clone 259D, BioLegend) or anti-granzyme B antibody (FITC, Clone QA16A02, BioLegend) (30 min, 4 °C). All analyzer data were collected on BD FACSymphony or Agilent NovoCyte Penteon instruments and analyzed using FlowJo (TreeStar) and BD FACSDiva software.

Antibody detection by enzyme-linked immunosorbent assay

For detection of influenza-specific antibodies, enzyme-linked immunosorbent assay (ELISA) plates (Costar) were coated with 0.1 µg per well of 2022–2023 Fluzone Quadrivalent inactivated influenza vaccine (Sanofi). For detection of autoantigen-specific antibodies, ELISA plates (Costar) were coated with 0.1 µg PR3, snRNP, core histone or dsDNA per well as the capture antigen. Plates were coated with capture antigen overnight, followed by blocking reagents for 2 h. Then, cell supernatants from tonsil culture were added to the coated, blocked plates. After the plates had been washed with washing buffer, horseradish peroxidase-conjugated anti-human secondary antibodies to IgM/IgG/IgA (Sigma) were added to the plate for 1 h, followed by TMB substrate solution (Thermo Scientific). Sulfuric acid was added to stop the reaction, and the plates were read at 450 nm.

Protein expression, purification and biotinylation

We performed protein production and purification for generating spheromers following a previous study[31]. Briefly, 20 ml of Expi293F cells were subcultured at a density of 3×10^6 viable cells per ml in Expi293 expression medium (Thermo Fisher Scientific) and transfected with expression plasmids using ExpiFectamine 293 transfection reagent according to the manufacturer's instructions. The cells were supplemented with enhancers after 18 h and further incubated for 4 days. The supernatant was collected by centrifugation (2,000*g*, 30 min, 4 °C) and gently mixed with buffer-equilibrated nickel-nitrilotriacetic acid (Ni-NTA) beads (Qiagen) overnight at 4 °C. Then, the Ni-NTA beads were collected and washed with 20 mM imidazole in HEPES-buffered saline (pH 7.2). The bound protein was eluted using 200 mM imidazole in HEPES-buffered saline (pH 7.2). The proteins were further purified using Amicon Ultra centrifugal units (Millipore Sigma) based on their molecular size. The eluted fractions were analyzed for purity using sodium dodecyl sulfate polyacrylamide gel electrophoresis. The protein was buffer-exchanged to remove the imidazole and biotinylated using a BirA biotin-protein ligase reaction kit (Avidity) according to the manufacturer's recommendations. The biotinylated proteins were subsequently purified using Amicon Ultra centrifugal units (Millipore Sigma) based on their molecular weight. The eluted fractions were analyzed for purity and biotinylation using sodium dodecyl sulfate polyacrylamide gel electrophoresis.

Assembly of the peptide-MHC–spheromer complex and autoantigen–spheromer complex

The assembly was started by generating a semisaturated SAv–peptide-MHC_2 ($pMHC_2$) complex. First, 1 µM pMHC-I monomers (NIH tetramer core facility), pMHC-I monomers (NIH tetramer core facility) or autoantigens (generated in-house) were incubated with 0.45 µM streptavidin–fluorophore (BioLegend) at a 1:0.45 ratio at room temperature for 30 min protected from light. The sequences of monomers are provided in Supplementary Table 2. Then, the mixture was incubated with an engineered maxi-ferritin scaffold[31] at room temperature for 1 h protected from light with gentle rotation. Molar excess of D-biotin was added to saturate any free biotin-binding sites on streptavidin of $pMHC_2$. The assembled spheromer was stored at 4 °C for later use.

Binding affinity measurement

The binding affinity of full-length H1 California/04/2009 influenza hemagglutinin (CA/09 HA) to the antibodies secreted into the culture media of the indicated human tonsil organoids on day 10 after LAIV stimulation was measured by biolayer interferometry using an Octet QK instrument (Pall ForteBio). The antigen (H1 CA/09 HA) diluted in PBST (PBS with 0.05% Tween 20, pH 7.4) was captured using Ni-NTA biosensors. The ligand-bound biosensors were dipped into a serially diluted culture supernatant. The association and dissociation were both monitored for 1 h. Double referencing was performed using unliganded biosensors and an irrelevant *Escherichia coli* maltose-binding protein. The $t_{1/2}$ was calculated from the off-rate (k_{off}) using the equation for first-order rate kinetics, $t_{1/2}2 = 0.693/k_{off}$. Each binding interaction was performed in duplicate.

Statistical analysis

Most statistical analyses except for those shown in Fig. 7 were performed using GraphPad Prism (v.10). All results are presented as mean ± s.e.m. The significance of the differences between groups were analyzed as described in the figure legends. To assess the relationship between autoantibody levels and donor age and sex, a linear regression analysis was conducted for each autoantibody (dsDNA, PR3, histone and snRNP). Optical density fold changes from ELISA assays were used as the response variable, with age and sex interaction terms as predictors. The model estimated the coefficients (slopes) for age effects in males and females separately. Model fit was evaluated using the *F*-statistic, *P* value and adjusted R^2 value. Statistical significance was determined for each predictor, and residuals were assessed for model accuracy. All analyses were performed using R.

Reporting summary

Further information on research design is available in the Nature Portfolio Reporting Summary linked to this article.

Data availability

All data are available in Figs. 1–7, Supplementary Information and Extended Data Figs. 1–7. Source data are provided with this paper.

Code availability

Code for statistical analysis using R and existing software packages has been described in the Methods section. No custom code was used in this study.

Acknowledgements

We thank all the volunteers and patients for their participation in this study. We also thank L. Chen and L. Kamalyan for tonsil processing, J. Li for providing the autoreactive peptides, the Stanford Shared FACS Facility for assistance in flow cytometric analysis, and D. Fernandez and O. N. Pattelli from Stanford ChEM-H Macromolecular Structure Knowledge Center for their guidance in protein production and purification. Finally, we thank the participants for donating their tissues for the tonsil organoids study. HLA typing was performed at the Stanford Functional Genomics Facility. This work was supported by the Lundbeck Foundation's Danish American Research Exchange

Fellowship to M.G. and grants from the Howard Hughes Medical Institute, Open Philanthropy, The Bill and Melinda Gates Foundation, and NIAID (AI057229) to M.M.D.

Author contributions

Project conceptualization and study design were performed by X.C. and M.M.D. Experiments were performed by X.C., M.G. and K.R.K. Data analyses were performed by X.C. and M.M.D. E.S. assisted with tonsil and peripheral blood mononuclear cell sample databases and data collection, processing and banking. V.M. performed the biolayer interferometry experiments and analysis. R.C. provided tonsil samples. X.C. and M.M.D. wrote the paper with input from all authors.

Competing interests

M.M.D., X.C., M.G. and V.M. are inventors on a patent application (PCT/US2023/010431) on the systems and methods incorporating modified T cells described in this work. The other authors declare no competing interests.

Additional information

Extended data is available for this paper at https://doi.org/10.1038/s41590-024-02062-x.

Supplementary information The online version contains supplementary material available at https://doi.org/10.1038/s41590-024-02062-x.

Correspondence and requests for materials should be addressed to Mark M. Davis.

Peer review information *Nature Immunology* thanks Bing Su and the other, anonymous, reviewer(s) for their contribution to the peer review of this work. Primary Handling Editor: S. Houston, in collaboration with the *Nature Immunology* team.

https://doi.org/10.1038/s41590-024-02062-x

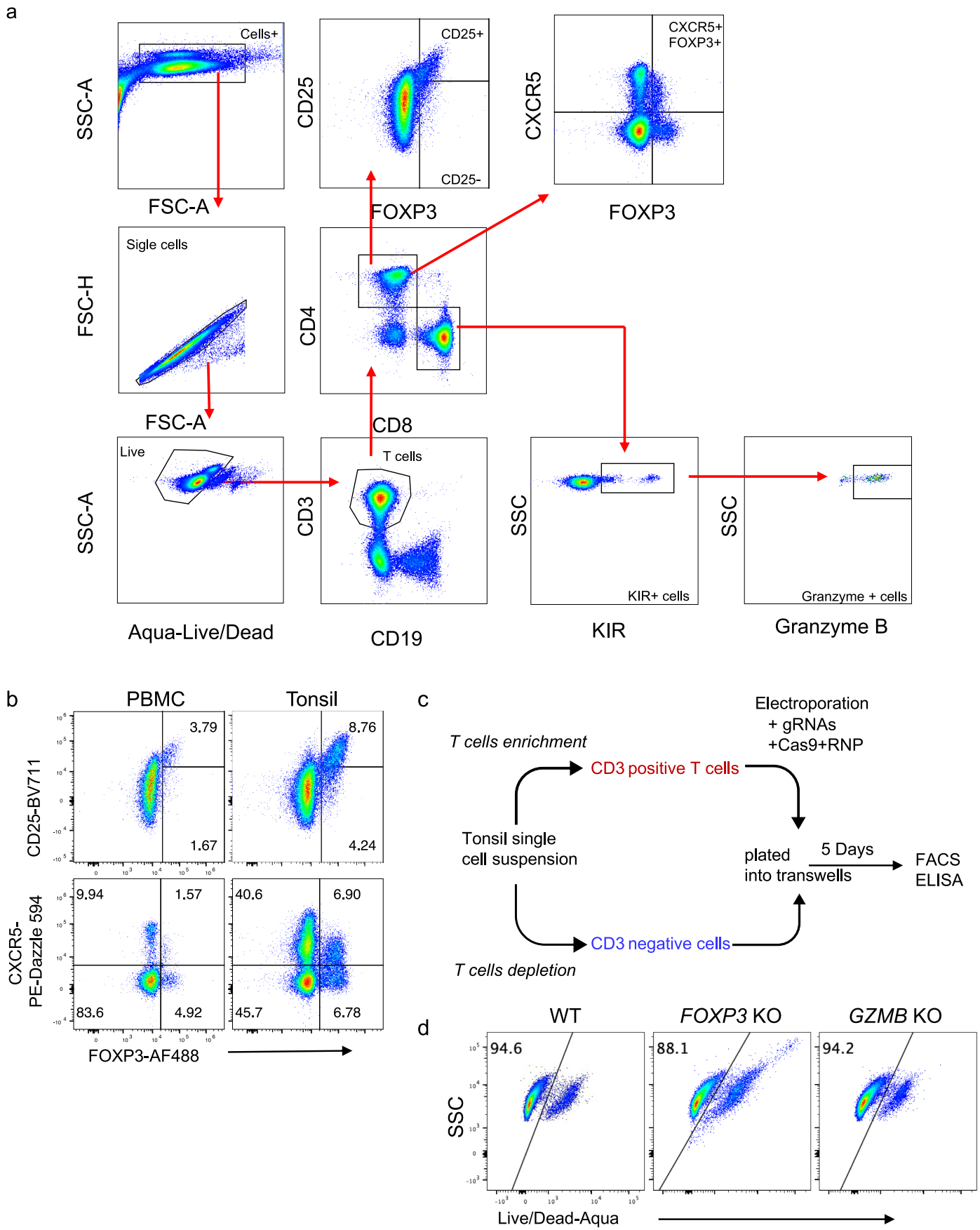

Extended Data Fig. 1 | The cell subset percentage and phenotypic differences in tonsils compared to donor-matched peripheral blood and viability after knockouts. a, A detailed flow gating strategy is used for the plots in Fig. 1a–c. **b**, A representative FACS profile showing CD25, CXCR5, and FOXP3 expression in PBMC and tonsil samples. **c**, A workflow of generating genetically modified tonsil organoids using Cas9-RNPs. **d**, A representative FACS profile showing Live/Dead staining of T cells from the WT, *FOXP3* KO, and *GZMB* KO tonsil organoids.

https://doi.org/10.1038/s41590-024-02062-x

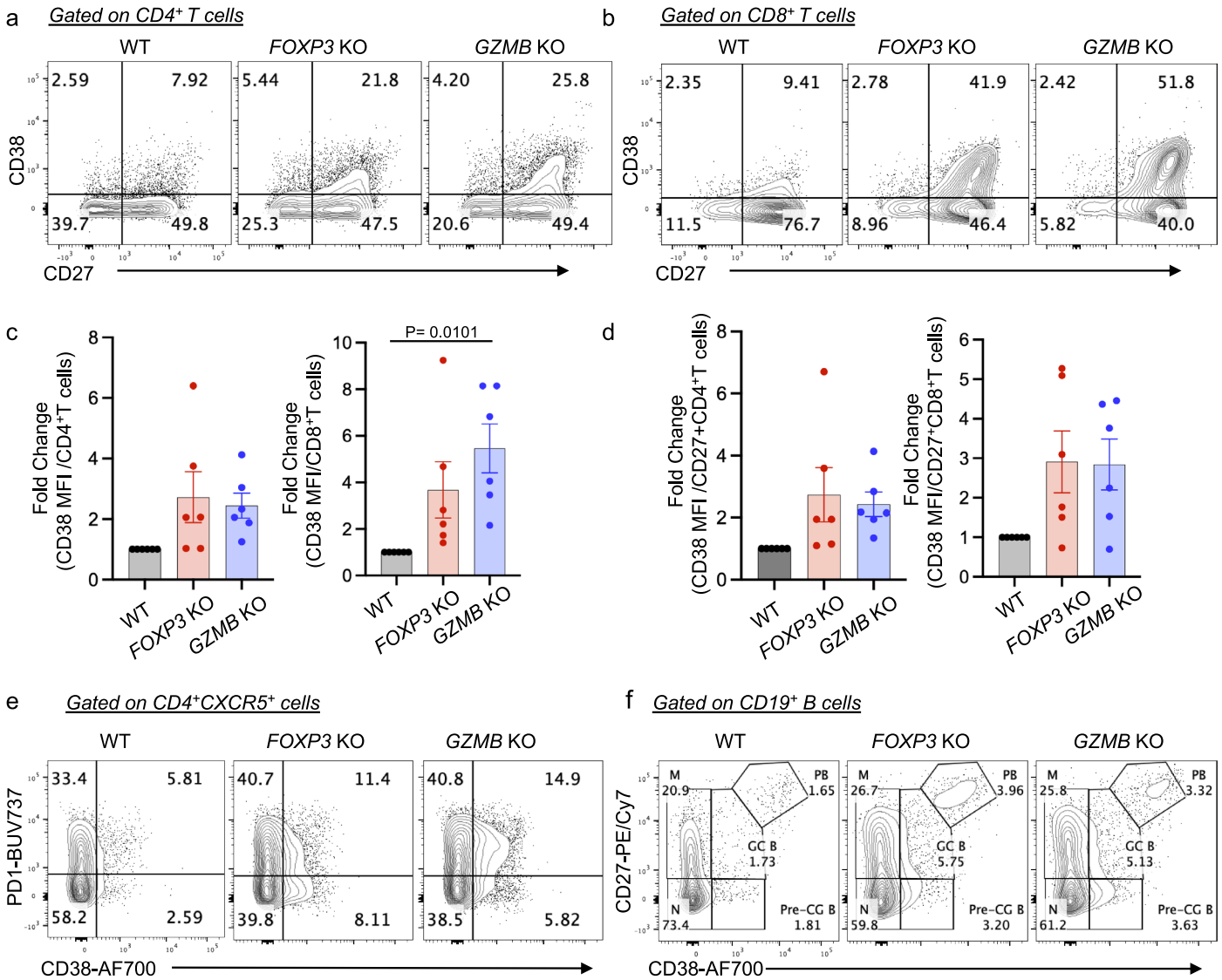

Extended Data Fig. 2 | Tonsil organoids with *FOXP3* KO and *GZMB* KO total T cells displayed inflammatory phenotypes after 5-day culture. **a, b**, Representative FACS plots showing the expression of CD38 and CD27 on $CD4^+$ T cells (**a**) and $CD8^+$ T cells (**b**) in organoids with WT, *FOXP3* KO, and *GZMB* KO T cells. **c, d** Statistical analysis of the fold change in CD38 MFI of $CD4^+$ T cells (**c**, left panel) and $CD8^+$ T cells (**c**, right panel), as well as $CD27^+CD4^+$ T cells (**d**, left panel) and $CD27^+CD8^+$ T cells (**d**, right panel) in organoids with WT, *FOXP3* KO, and *GZMB* KO T cells (n = 6). **e** Representative FACS plots showing the expression of PD1 and CD38 on Tfh cells (pre-gated on $CD4^+$ $CXCR5^+$) in WT and KO tonsil organoids after 5-day culture without stimulation. **f**, Representative FACS plot showing the expression of CD27 and CD38 on B cells (pre-gated on $CD3^-CD19^+$) in WT and KO tonsil organoids after 5-day culture without stimulation. The significance in (**c**) and (**d**) was calculated by one-way ANOVA followed by Tukey's multiple comparisons test.

https://doi.org/10.1038/s41590-024-02062-x

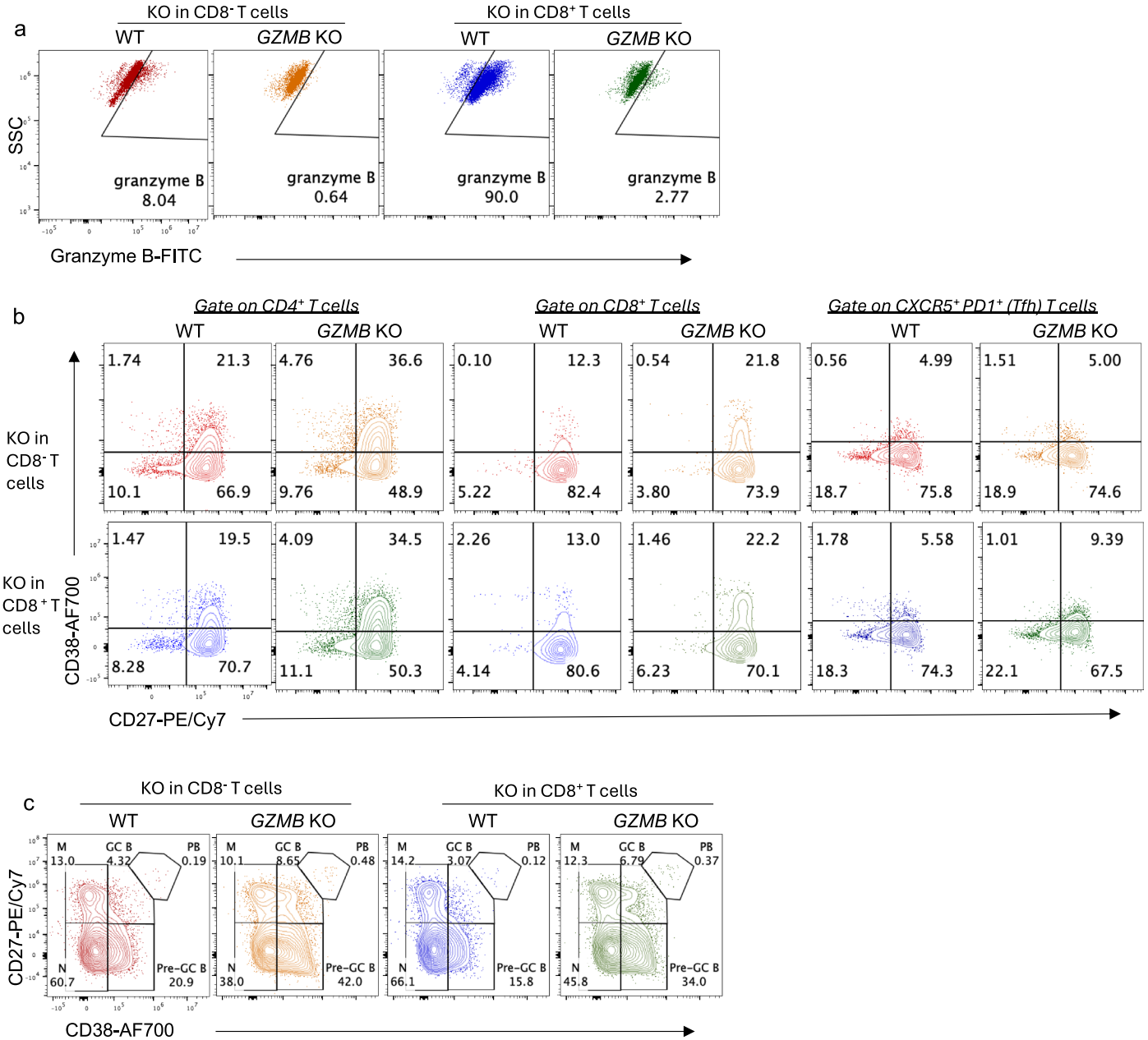

Extended Data Fig. 3 | Representative plots showing inflammatory phenotypes in tonsil organoids with GZMB KO in CD8⁺ and CD8⁻ T cells. **a**, Granzyme B expression in CD8⁻ and CD8⁺ T cells 5 days post GZMB KO. **b**, Expression of CD38 and CD27 in CD4⁺ T cells, CD8⁺ T cells and Tfh cells from 5-day cultured tonsil organoids with GZMB KO in CD8⁻ and CD8⁺ T cells. **c**, Expression of CD27 and CD38 in B cells from tonsil organoids with GZMB KO in CD8⁻ and CD8⁺ T cells.

https://doi.org/10.1038/s41590-024-02062-x

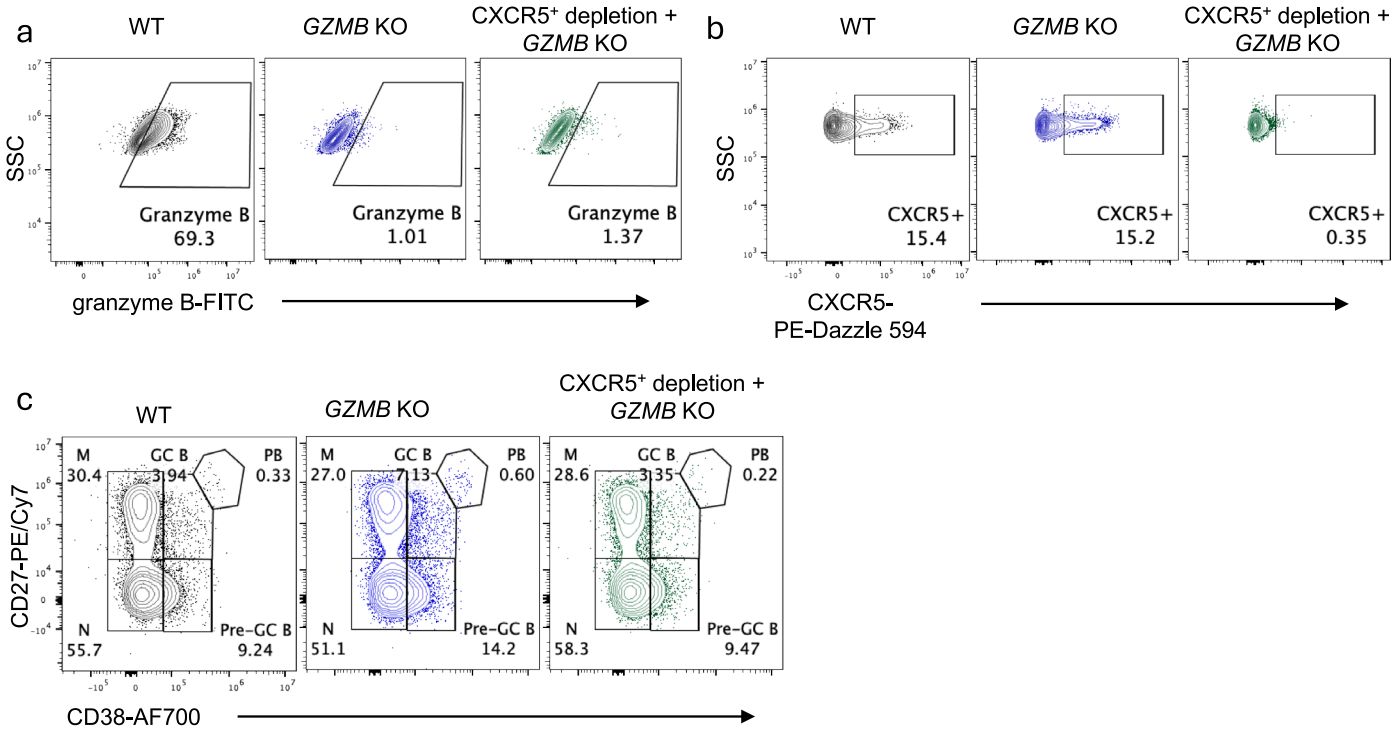

Extended Data Fig. 4 | Representative plots showing plasmablast differentiation after CXCR5$^+$ depletion and GZMB KO in CD8$^+$ T cells of tonsil organoids. a, Granzyme B expression in CD8$^+$ T cells under the indicated conditions from tonsil organoids. **b**, CXCR5 expression in CD4$^+$ T cells under indicated conditions from tonsil organoids. **c**, Expression of CD27 and CD38 in B cells from tonsil organoids with WT, GZMB KO, and CXCR5-depleted GZMB KO CD8$^+$ T cells.

https://doi.org/10.1038/s41590-024-02062-x

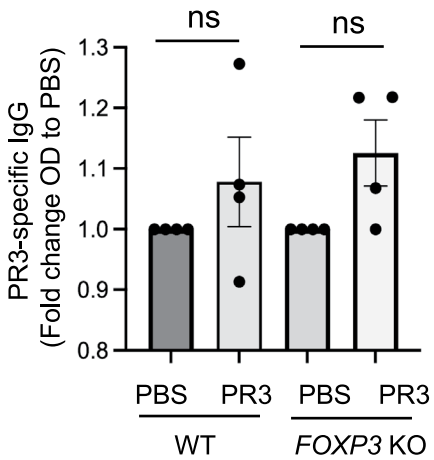

Extended Data Fig. 5 | PR3-Specific Autoantibody Production in Organoids with WT or *FOXP3* KO T Cells. Ten-day cell supernatant from organoids with WT or *FOXP3* KO T cells w as collected, and PR3-specific autoantibody was measured by ELISA (n = 4). The fold change in PR3-specific antibody (OD) between PBS and PR3 conditions was calculated. Significance was determined using one-way ANOVA followed by Tukey's multiple comparisons test. ns, not significant.

https://doi.org/10.1038/s41590-024-02062-x

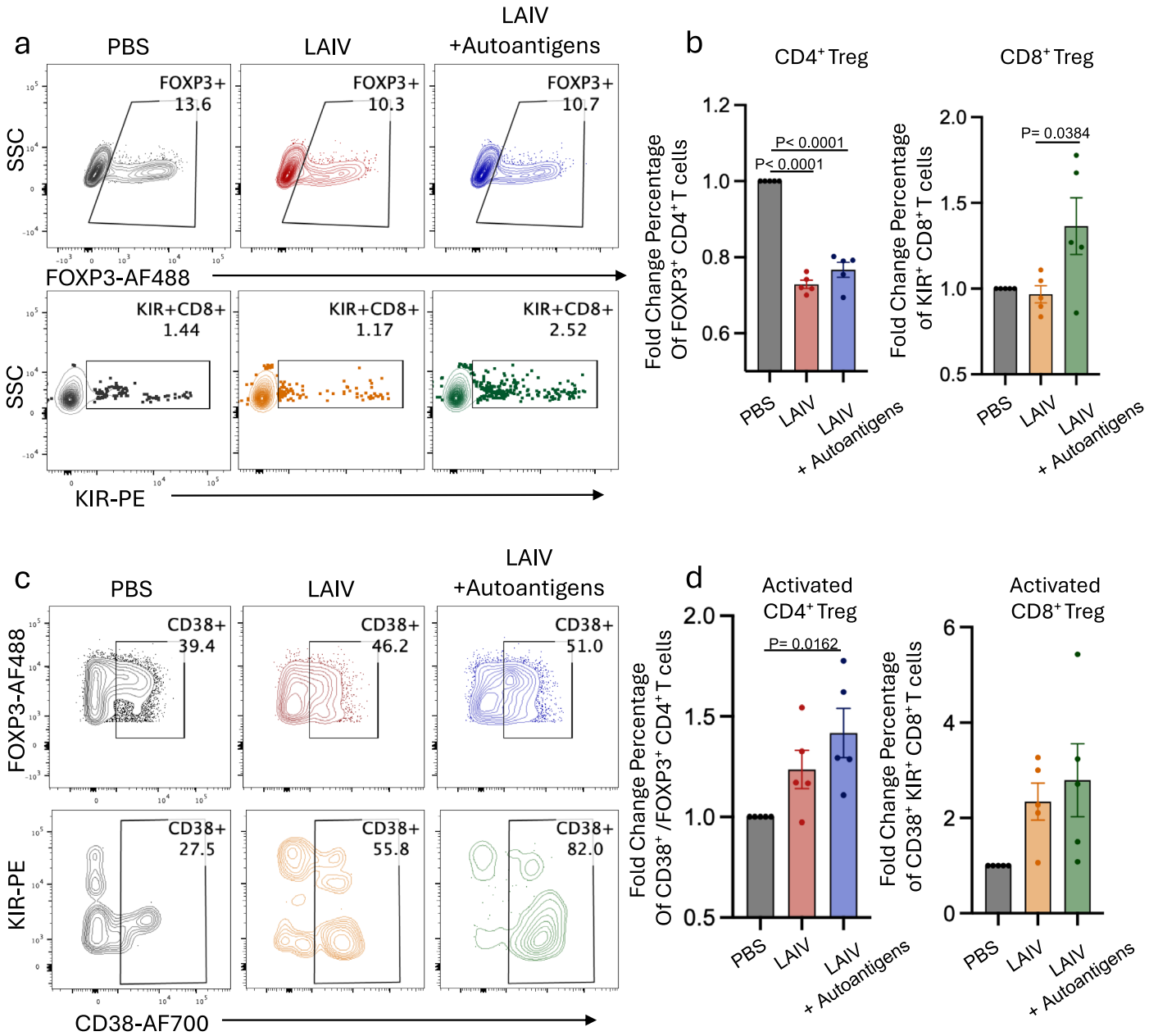

Extended Data Fig. 6 | CD4$^+$ and CD8$^+$ Tregs markers and phenotypes in WT organoids stimulated with LAIV or LAIV plus autoantigens. a, Representative FACS plots showing CD4$^+$ Tregs (*FOXP3*$^+$ in CD4$^+$ T cells) or CD8$^+$ Tregs (KIR$^+$ in CD8$^+$ T cells) in WT tonsil organoids after 5 days of culture. **b**, Fold change in the percentage of FOXP3$^+$CD4$^+$ T cells and KIR$^+$CD8$^+$ T cells in WT tonsil organoids stimulated with LAIV or LAIV plus autoantigens (n = 5 donors). **c**, Representative FACS plots showing CD38 expression on CD4$^+$ Tregs (pre-gated on FOXP3$^+$CD4$^+$ T cells) or KIR$^+$CD8$^+$ Tregs (pre-gated on KIR$^+$CD8$^+$ T cells) in WT tonsil organoids after 5 days of culture. **d**, Fold change in the percentage of activated CD38$^+$ FOXP3$^+$CD4$^+$ T cells and CD38$^+$ KIR$^+$CD8$^+$ T cells in WT tonsil organoids stimulated with LAIV or LAIV plus autoantigens (n = 5 donors). Significance in (**b**) and (**d**) was calculated by one-way ANOVA followed by Tukey's multiple comparisons test.

https://doi.org/10.1038/s41590-024-02062-x

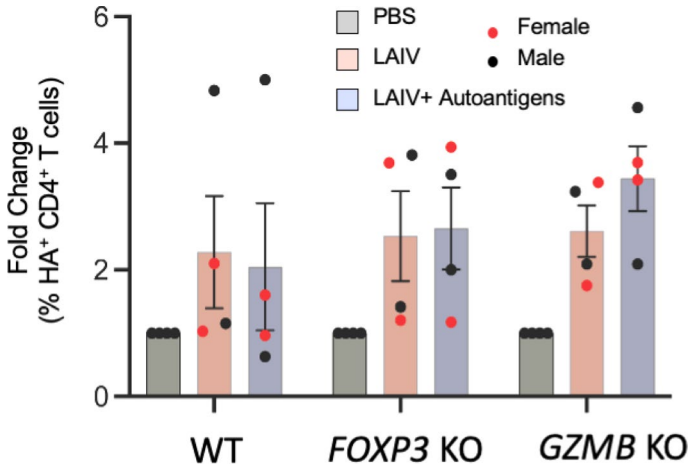

Extended Data Fig. 7 | The percentage of HA-specific CD4$^+$ T cells in organoids with WT, *FOXP3* KO, or *GZMB* KO T cells. HLA-DRB1*04:01 tonsil organoids with WT, *FOXP3 KO* or *GZMB* KO total CD3$^+$ T cells (n = 4 donors) were cultured for 7 days, followed by staining with HA-specific spheromer. The fold change in the percentage of HA-specific CD4$^+$ T cells relative to the PBS condition was calculated. Mean ± s.e.m is indicated. Significances were calculated by two-way ANOVA followed by Tukey's multiple comparisons test. All p-values are greater than 0.05.

nature portfolio

Corresponding author(s): Mark M Davis

Last updated by author(s): 2024/12/05

Reporting Summary

Nature Portfolio wishes to improve the reproducibility of the work that we publish. This form provides structure for consistency and transparency in reporting. For further information on Nature Portfolio policies, see our Editorial Policies and the Editorial Policy Checklist.

Statistics

For all statistical analyses, confirm that the following items are present in the figure legend, table legend, main text, or Methods section.

n/a	Confirmed	
☐	☒	The exact sample size (*n*) for each experimental group/condition, given as a discrete number and unit of measurement
☐	☒	A statement on whether measurements were taken from distinct samples or whether the same sample was measured repeatedly
☐	☒	The statistical test(s) used AND whether they are one- or two-sided *Only common tests should be described solely by name; describe more complex techniques in the Methods section.*
☒	☐	A description of all covariates tested
☐	☒	A description of any assumptions or corrections, such as tests of normality and adjustment for multiple comparisons
☐	☒	A full description of the statistical parameters including central tendency (e.g. means) or other basic estimates (e.g. regression coefficient) AND variation (e.g. standard deviation) or associated estimates of uncertainty (e.g. confidence intervals)
☐	☒	For null hypothesis testing, the test statistic (e.g. *F*, *t*, *r*) with confidence intervals, effect sizes, degrees of freedom and *P* value noted *Give P values as exact values whenever suitable.*
☒	☐	For Bayesian analysis, information on the choice of priors and Markov chain Monte Carlo settings
☒	☐	For hierarchical and complex designs, identification of the appropriate level for tests and full reporting of outcomes
☒	☐	Estimates of effect sizes (e.g. Cohen's *d*, Pearson's *r*), indicating how they were calculated

Our web collection on statistics for biologists contains articles on many of the points above.

Software and code

Policy information about availability of computer code

Data collection	Flow cytometry date were collected using BD FACSDiva software (v7). FACS data were obtained using BD FACSymphony or Agilent NovoVyte Penteon instruments.
Data analysis	FlowJo 10.7.0 was used for the analysis of flow cytometry data. GraphPad Prism 10.1 and R studio 4.0.3 were used for plotting and statistical analysis.

For manuscripts utilizing custom algorithms or software that are central to the research but not yet described in published literature, software must be made available to editors and reviewers. We strongly encourage code deposition in a community repository (e.g. GitHub). See the Nature Portfolio guidelines for submitting code & software for further information.

Data

Policy information about availability of data

All manuscripts must include a data availability statement. This statement should provide the following information, where applicable:

- Accession codes, unique identifiers, or web links for publicly available datasets
- A description of any restrictions on data availability
- For clinical datasets or third party data, please ensure that the statement adheres to our policy

All data are available in the figures, text, and supplementary figures, with source data.

Research involving human participants, their data, or biological material

Policy information about studies with human participants or human data. See also policy information about sex, gender (identity/presentation), and sexual orientation and race, ethnicity and racism.

Reporting on sex and gender	Both male and female patients are reported. Sex information was obtained from electronic patient records, with informed consent collected from all participants. The patients' ages range from 4 to 66 years, with 64% of the cohort being male and 36% female. Sex data was provided in the source data
Reporting on race, ethnicity, or other socially relevant groupings	Race and ethnicity data are listed in the supplementary information
Population characteristics	Patients undergoing tonsillectomy were recruited with IRB approval for donating tissues to this study. Patients with serious infections or who were taking systemic immunomodulatory drugs were excluded from the study. The patients' ages range from 4 to 66 years, with 64% of the cohort being male and 36% female.
Recruitment	Patients will be referred to the appropriate clinical units for their respective care, such as surgical procedures. Prior to the patient's surgery, our research team will contact the family of the child or adult patient to obtain written informed consent. Patients with serious infections or who were taking systemic immunomodulatory drugs were excluded from the study. Individiuals responsible for consenting patients and collecting tissues were not involved in the scientific aspects of the study. We do not expect any systematic bias in our collection strategy.
Ethics oversight	The collection and process of tonsil samples from children and adult volunteers were covered by IRB protocols 30837 and 60741, approved by the Stanford University Institutional Review Board (IRB). Informed consents were obtained from the participants and/or from parents/legal guardians. No participant compensation was provided for the participants. Blood from healthy donors was requested from the Stanford Blood Center under IRB protocol 40146.

Note that full information on the approval of the study protocol must also be provided in the manuscript.

Field-specific reporting

Please select the one below that is the best fit for your research. If you are not sure, read the appropriate sections before making your selection.

☒ Life sciences ☐ Behavioural & social sciences ☐ Ecological, evolutionary & environmental sciences

For a reference copy of the document with all sections, see nature.com/documents/nr-reporting-summary-flat.pdf

Life sciences study design

All studies must disclose on these points even when the disclosure is negative.

Sample size	Sample sizes varied from n=4 to n=15 depending on the experiments performed. Sample size was based on previous expeiments (PMID: 33432170) and clinical samples availability.
Data exclusions	No data were excluded
Replication	The number of donors tested is provided in the figure legends. We anticipated inter-donor variation in response to the stimulation and treatment and responses to stimulation were reported in figures or in text. Different donors were used to demonstrate the range of possible responses.
Randomization	Experimental groups were stimulation-related, sex and age-related, thus randomization is not relevant.
Blinding	Blinding is irrelevant for this study as it is not a clinical trial. The objective is to assess cell culture responses to various treatments using established assays.

Reporting for specific materials, systems and methods

We require information from authors about some types of materials, experimental systems and methods used in many studies. Here, indicate whether each material, system or method listed is relevant to your study. If you are not sure if a list item applies to your research, read the appropriate section before selecting a response.

Materials & experimental systems

n/a	Involved in the study
☐	☒ Antibodies
☐	☒ Eukaryotic cell lines
☒	☐ Palaeontology and archaeology
☒	☐ Animals and other organisms
☒	☐ Clinical data
☒	☐ Dual use research of concern
☒	☐ Plants

Methods

n/a	Involved in the study
☒	☐ ChIP-seq
☐	☒ Flow cytometry
☒	☐ MRI-based neuroimaging

Antibodies

Antibodies used

anti-human CD3 (BUV805) 1/50 BD Biosciences Cat# 612895; RRID:AB_2870183
anti-human CD19 (BUV737) 1/50 BioLegend Cat# 741829; RRID:AB_2871164
anti-human CD4 (BV650) 1/50 BioLegend Cat# 317436; RRID:AB_2563050
anti-human CD8 (BV421) 1/50 BioLegend Cat# 301036; RRID:AB_10960142
anti-human CXCR5 (PE-Dazzle 594) 1/50 BioLegend Cat# 356928; RRID:AB_2563689
anti-human PD1 (APC) 1/20 BioLegend Cat# 329908; RRID:AB_940475
anti-human CD38 (Alexa Fluor 700) 1/100 BioLegend Cat# 303524; RRID:AB_2072781
anti-human CD27 (Pecy7) 1/100 BioLegend Cat# 302838; RRID:AB_2561919
anti-human CD158e1 (KIR3DL1) (PE) 1/50 BioLegend Cat# 312708; RRID:AB_2249498
anti-human CD158b (KIR2DL2/L3, NKAT2) (PE) 1/100 BioLegend Cat# 312606; RRID:AB_2130554
anti-human CD158f (KIR2DL5) Antibody (PE) 1/100 BioLegend Cat# 341304; RRID:AB_2130701
anti-FOXP3 (Alexa Fluor 488) 1/50 BioLegend Cat# 320212; RRID:AB_430887
anti-FOXP3 (Alexa Fluor 647) 1/50 BioLegend Cat# 320214; RRID:AB_492984
anti-granzyme B (FITC) 1/100 BioLegend Cat# 372206; RRID:AB_2687030
anti-human CD25 (BV711) 1/50 BioLegend Cat# 356138; RRID:AB_2632781
anti-human CD8 (PE) 1/10 BioLegend Cat#; 344706; RRID:AB_1953244
anti-human CXCR5 (PE) 1/25 BioLegend Cat# 356904; RRID:AB_2561813

Validation

All antibodies were purchased from commercial suppliers (BD Biosciences, BioLegend, ThermoFisher). Validation statement were confirmed from the manufacturers' website for their relevant used in the study:
anti-human CD3 (BUV805) https://www.bdbiosciences.com/en-us/products/reagents/flow-cytometry-reagents/research-reagents/single-color-antibodies-ruo/buv805-mouse-anti-human-cd3.612895
anti-human CD19 (BUV737) https://www.bdbiosciences.com/en-us/resources/scientific-resources?resourceType::all=all
anti-human CD4 (BV650) https://www.biolegend.com/en-ie/products/brilliant-violet-650-anti-human-cd4-antibody-7786?GroupID=BLG5901
anti-human CD8 (BV421) https://www.biolegend.com/en-ie/products/brilliant-violet-421-anti-human-cd8a-antibody-7152
anti-human CXCR5 (PE-Dazzle 594) https://www.biolegend.com/en-ie/products/pe-dazzle-594-anti-human-cd185-cxcr5-antibody-9860
anti-human PD1 (APC) https://www.biolegend.com/en-ie/products/apc-anti-human-cd279-pd-1-antibody-4413
anti-human CD38 (Alexa Fluor 700) https://www.biolegend.com/en-ie/products/alexa-fluor-700-anti-human-cd38-antibody-6050
anti-human CD27 (Pecy7) https://www.biolegend.com/en-us/products/pe-cyanine7-anti-human-cd27-antibody-8434
anti-human CD158e1 (KIR3DL1) (PE) https://www.biolegend.com/en-us/products/pe-anti-human-cd158e1-kir3dl1-nkb1-antibody-2286
anti-human CD158b (KIR2DL2/L3, NKAT2) (PE) https://www.biolegend.com/en-us/products/pe-anti-human-cd158b-j-kir2dl2-l3-s2-antibody-2281
anti-human CD158f (KIR2DL5) Antibody (PE) https://www.biolegend.com/en-us/products/pe-anti-human-cd158f-kir2dl5-antibody-5809
anti-FOXP3 (Alexa Fluor 488) https://www.biolegend.com/en-us/products/alexa-fluor-488-anti-human-foxp3-antibody-2908
anti-FOXP3 (Alexa Fluor 647) https://www.biolegend.com/en-us/products/alexa-fluor-647-anti-human-foxp3-antibody-2909
anti-granzyme B (FITC) https://www.biolegend.com/en-us/products/fitc-anti-human-mouse-granzyme-b-recombinant-antibody-14430
anti-human CD25 (BV711) https://www.biolegend.com/en-us/products/brilliant-violet-711-anti-human-cd25-antibody-13762
anti-human CD8 (PE) https://www.biolegend.com/en-us/products/pe-anti-human-cd8-antibody-6247
anti-human CXCR5 (PE) https://www.biolegend.com/en-us/products/pe-anti-human-cd185-cxcr5-antibody-8358

Eukaryotic cell lines

Policy information about cell lines and Sex and Gender in Research

Cell line source(s)	Expi293F Cells from thermofisher (cat# A14527)
Authentication	Identity of the cell lines were frequently checked by their morphological features
Mycoplasma contamination	Mycoplasma contamination was tested negative for mycoplasma via qPCR performed by ThermoFisher

Commonly misidentified lines (See ICLAC register)	No commonly misidentified cell lines are used in this study

Plants

Seed stocks	N/A
Novel plant genotypes	N/A
Authentication	N/A

Flow Cytometry

Plots

Confirm that:

☒ The axis labels state the marker and fluorochrome used (e.g. CD4-FITC).

☒ The axis scales are clearly visible. Include numbers along axes only for bottom left plot of group (a 'group' is an analysis of identical markers).

☒ All plots are contour plots with outliers or pseudocolor plots.

☒ A numerical value for number of cells or percentage (with statistics) is provided.

Methodology

Sample preparation	Culture organoids were resuspended by rinsing the membrane with media and collected from the transwells. Cells were washed with FACS buffer (PBS+0.1% BSA, 0.05% sodium azide and 2 mM EDTA) and treated with Fc receptor block (Biolegend, 10ug/ml) in FACS buffer for 10 mins followed by staining with live/dead Aqua Zombie stain (1/100), and antibodies against surface markers (30min, 4°C). For intracellular staining, the cells were fixed and permeabilized followed by staining with anti-FOXP3 or anti-granzyme B antibody (30min, 4°C).
Instrument	FACS data were obtained using BD FACSymphony or Agilent NovoVyte Penteon instruments. BD FACSAria was used for Cell sorting
Software	Flow cytometry date were collected using BD FACSDiva software (v7).
Cell population abundance	The purify of the sorted cells was more than 95%
Gating strategy	For generating the plots in Fig. 1, we began by excluding debris through gating on FSC-A vs. SSC-A. Next, we gated for single cells using a diagonal plot of FSC-A versus FSC-H to remove doublets, followed by selecting live cells by gating the negative population from the Live/Dead stain. We then identified CD3+ T cells, distinguishing them from non-T cells by excluding CD19 + B cells. At this stage, we separated the two main T cell subsets, CD4+ and CD8+ T cells, into distinct populations using a CD4 vs. CD8 plot. To identify the percentage of CD4+ Tregs as shown in Fig 1(A, left panel), we gated on total FOXP3+ cells within the CD4+ population. The percentage of the CD25- population in Fig 1(A, right panel) was further determined by gating on the CD25 negative population from FOXP3+CD4+ T cells. To determine the percentage of T Follicular Regulatory cells, we examined the percentage of CXCR5 and FOXP3 double-positive cells from CD4+ T cells. Within the CD8+ T cell population, we identified CD8+ Tregs based on the expression of KIR (Killer Immunoglobulin-like Receptor), which defines a regulatory subset within CD8+ T cells. Finally, we assessed the Granzyme B expression in these KIR + CD8+ Tregs.

☒ Tick this box to confirm that a figure exemplifying the gating strategy is provided in the Supplementary Information.